Understanding Filter Induced Star Halos

by Jim Thompson, P.Eng

Test Report – November 24th, 2022

Abstract

This report documents a series of experiments and analyses that I have performed in an attempt to understand how the properties of an astronomical filter affect the extent to which the filter produces halos around bright stars. Aspects of the problem that were investigated include: the types of stars prone to filter induced halos, the distance of the filter from the sensor, the focal ratio of the telescope, quantitative evaluation of halo production by a large sample of filter types, measurement of filter spectral reflectivity, measurement of filter off-band blocking, analysis of correlation between filter properties, and numerical simulation of halo generation.

The following conclusions regarding the behaviour of filter induced star halos have been drawn from the various experiments and analyses summarized in this report:

1. The primary cause of filter induced star halos is intra-filter reflections.
2. The angular size of the halo is dependant only on the thickness of the filter glass and the telescope focal ratio. Filter distance from the sensor has no impact on the visibility or size of the halo.
3. For stars of the same visual magnitude, filters are more prone to generating halos around hot blue and cool red stars than moderate temperature orange, yellow, and white stars.
4. Filter off-band blocking performance is the primary characteristic affecting halo generation.
5. The use of anti-reflective coatings can help to reduce halos, but it is a lower magnitude impact compared to off-band blocking.

Table of Contents

1.0 Introduction

Astronomical filters can improve the quality of our observing or imaging efforts. They increase the contrast of the object we are trying to observe, and correspondingly increase the signal-to-noise ratio of our images. These qualities I have documented numerous times in the test reports authored up to this point. One characteristic of filters I have not discussed is their undesirable tendency to generate optical artifacts. By adding a filter to our telescope setups, we are adding two new surfaces for dirt and dust to collect, or for a reflection to occur. The later phenomenon is what is discussed in this report, reflections off filters. More specifically this report summarizes my investigation into the origin and nature of halos around bright stars caused by the presence of a filter.

1.1 Background

Prior to the effort documented here, I had not paid much attention to star halos. From the perspective of someone who observes through the use of Electronically Assisted Astronomy (EAA), the presence of halos around bright stars is just one of several image artifacts that have come to be accepted as part of the EAA process. Through my recent comparison testing of very narrowband filters it has come to my attention that halos, or rather their absence, can sometimes be the deciding factor for astrophotographers on whether to purchase one filter over another. For this reason I decided to have a more thorough look at the problem.

To start, it is important to come to a consensus on what people are calling a "halo". Figure 1 presents several images of bright stars with different types of artifacts around them. In many cases there are more than one type of artifact present in the image. Halos are defined as clearly delineated disks, relatively small in angular size, around bright stars. They are typically centered on the star but can be offset slightly when the star is at the edge of the field of view. Depending on the star brightness and other factors, there may be multiple concentric halos that both increase in diameter and decrease in brightness by a regular interval. Images a), b), c) and h) in Figure 1 all show evidence of a halo. The randomly distributed spikes around the star in images a), b), c), and e) are a result of small imperfections in the primary optics of the scope used to capture the image and are unrelated to the presence of a filter. The bright symmetrical spikes in images b), d), and f) are diffraction spikes caused by the scope's secondary mirror supports, and in image h) is caused by a spider's web spanning across the inside of the optical tube. Images e), g), and h) all show a diffuse symmetrical 4-lobbed pattern around the bright star which is another artifact caused by the primary optics, not related to the filter. Finally, images f) and g) both show a large disk that is off center from the bright star. These are ghost images; reflections coming from the primary optics of the scope that the filter may also play a role in.

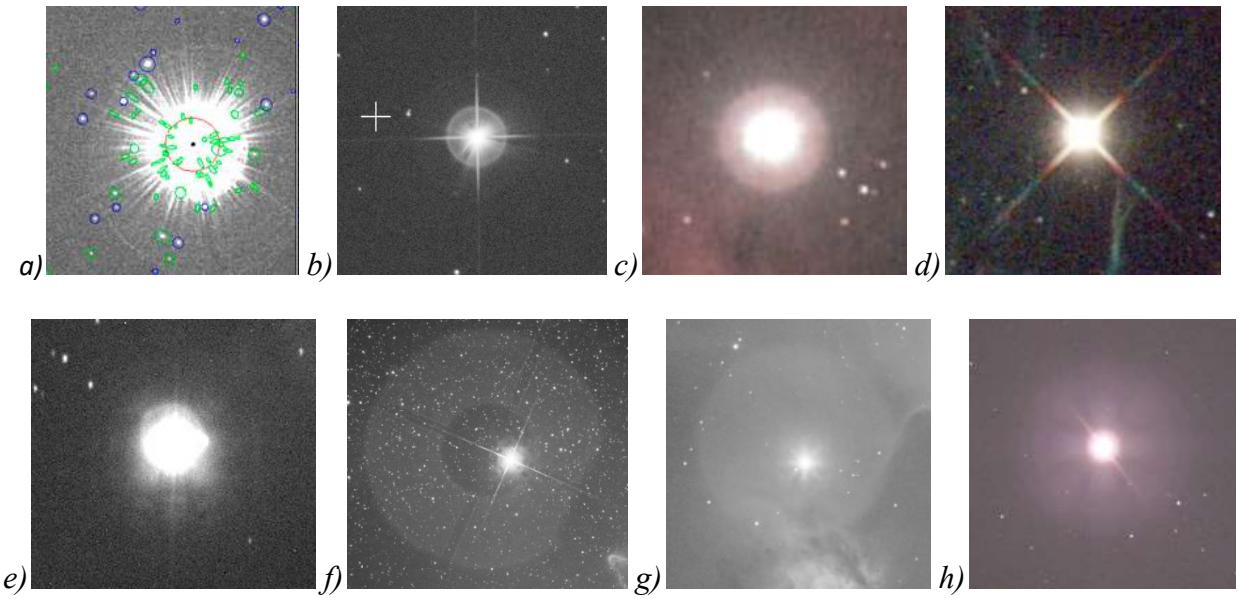

a) Findlay [6], b) Todd [4], c)-e) Thompson, f)-g) Jorksveld [7], h) Thompson

Figure 1 Star Images from Various Sources Illustrating Artefacts

Halos are typically small and centered on the star. Based on information I could find online, halos are believed to be due to a reflection that occurs between the filter and camera, or within the filter itself. When there is a focal reducer or field flattener present, it can also result in reflections and thus halos or ghost images depending on what the component is reflecting. For this report I consider halos generated without the presence of a focal reducer.

Figure 2 illustrates schematically the components of the optical train considered in my research, and how they might contribute to the generation of a halo or ghost. Reflections from the scope side of the filter, if they are able to somehow make their way back to the sensor, are responsible for large ghost images like those in images f) and g) in Figure 1. Reflections from the sensor side of the filter are also able to generate ghosts depending on scope focal ratio, how close the filter is to the sensor, and whether there is additional optics in the path between filter and sensor. Intra-filter reflections result in relatively small sized artifacts (i.e. halos) around stars, their angular size dependant only on the focal ratio of the scope and the thickness of the filter glass. Based on the geometric arrangement described in Figure 2, the size and brightness of the intra-filter reflection caused halo does not depend on how far the filter is from the camera. This is a property that I confirm by test later in this report.

The rest of this report documents a series of experiments I have performed, each one meant to garner some understanding of a particular aspect of the halo problem. The results from the earlier tests tended to point me in a certain direction for the following tests, and in some cases to completely change tact. The following sections are presented in the order in which the experiments were performed.

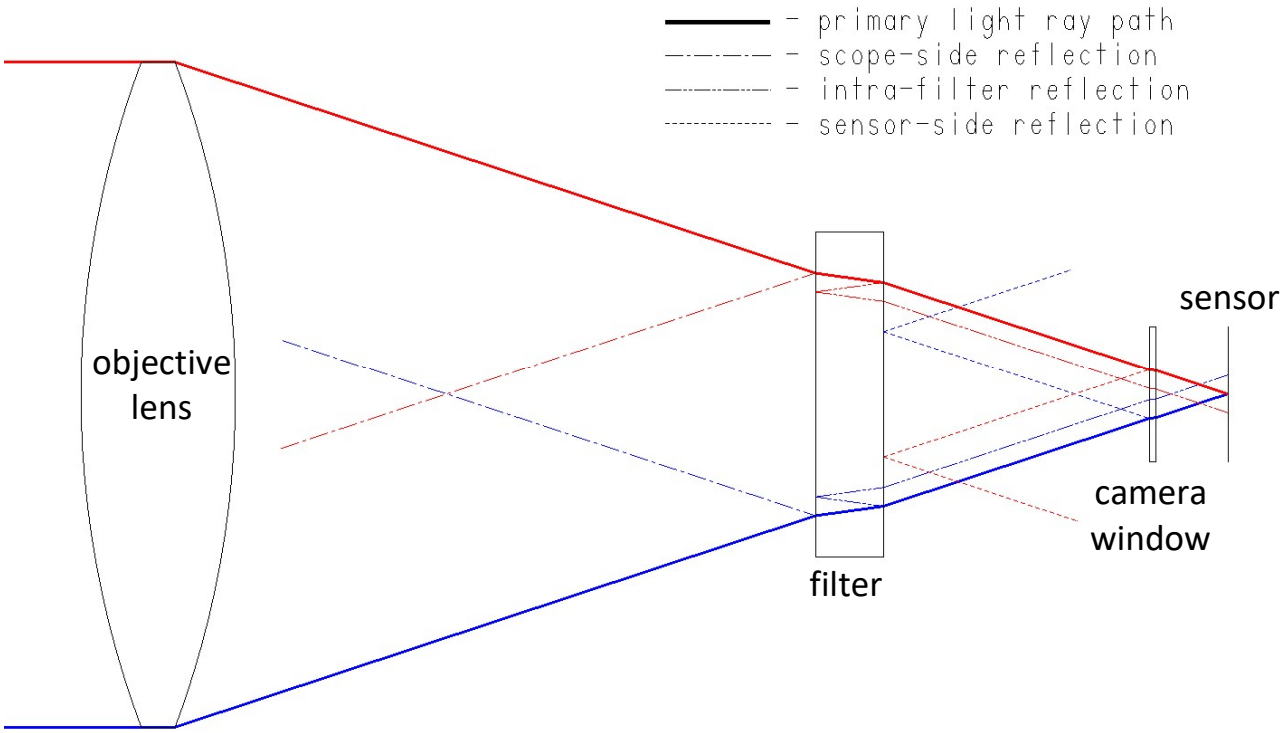

Figure 2 Schematic View of Typical Telescope-Filter-Camera Arrangement

1.2 References

1. Risch, Michael; "Halos - Viewed Without Prejudice", Baader Planetarium blog; 19-Dec-2019; https://www.baader-planetarium.com/en/blog/halos-viewed-without-prejudice/
2. Baader Planetarium; "Problems With Filters Can Have the Strangest Causes"; website FAQ; 2017; https://www.baader-planetarium.com/en/downloads/dl/file/id/287/product/4184/faq_problems_with_filters_can_have_the_strangest_causes.pdf
3. Astronomik; "Halos Around Bright Stars", website news; https://www.astronomik.com/en/news/astronomik_halo_free_filter_halo_problem/
4. Todd, Simon; "The Source to the Halo Around Bright Stars"; Simon Todd Astrophotography website; 20-Apr-2019; https://www.stastrophotography.com/the-source-to-the-halo-around-bright-stars/
5. Cambridge Astronomical Survey Unit; "Spikes and Halos"; VISTA survey project website; http://casu.ast.cam.ac.uk/surveys-projects/vista/technical/spikes-and-halos
6. Findlay, Joseph; "First Results from High Redshift Quasar Searches in VIKING"; PhD thesis submitted to University of London; June-2012; https://qmro.qmul.ac.uk/xmlui/handle/123456789/7558
7. Jorksveld, Ruben; "What Caused These Relfections? And What To Do?"; Cloudy Nights Forum; 23-Nov-2019; https://www.cloudynights.com/topic/684719-what-caused-these-relfections-and-what-to-do/#entry9788684

2.0 Types of Stars That Cause Halos

The first investigation I performed was to comb through my library of past image captures in search of images with star halos and determine the properties of the particular stars that displayed the halos. A few prominent examples that I found are shown in Figure 3. Not all stars generate visible halos, and some stars are worse than others. In general, the stars with halos are bright, generally the brightest star in the frame, but that is not always the case. A consistent property of stars that tend to have halos is that they are hot. Table 1 summarizes the properties of the stars I found in my images containing halos. In more than half of the cases the halo bearing stars are very hot, 8,000K or higher. The implication of this observation is that the emission spectrum of the star, which is defined by its temperature, has an effect on the extent to which a filter generates a halo. Figure 4 illustrates how the emission spectrum of a star changes with its temperature. The spectra in Figure 4 are scaled so that the overall visual brightness of the stars is the same. The figure shows that hot stars have their emissions biased towards the violet end of the spectrum, and cool stars are biased towards the red end. It stands to reason then that a filter designed to minimize halos around cooler stars might not perform well on hot stars, and visa versa.

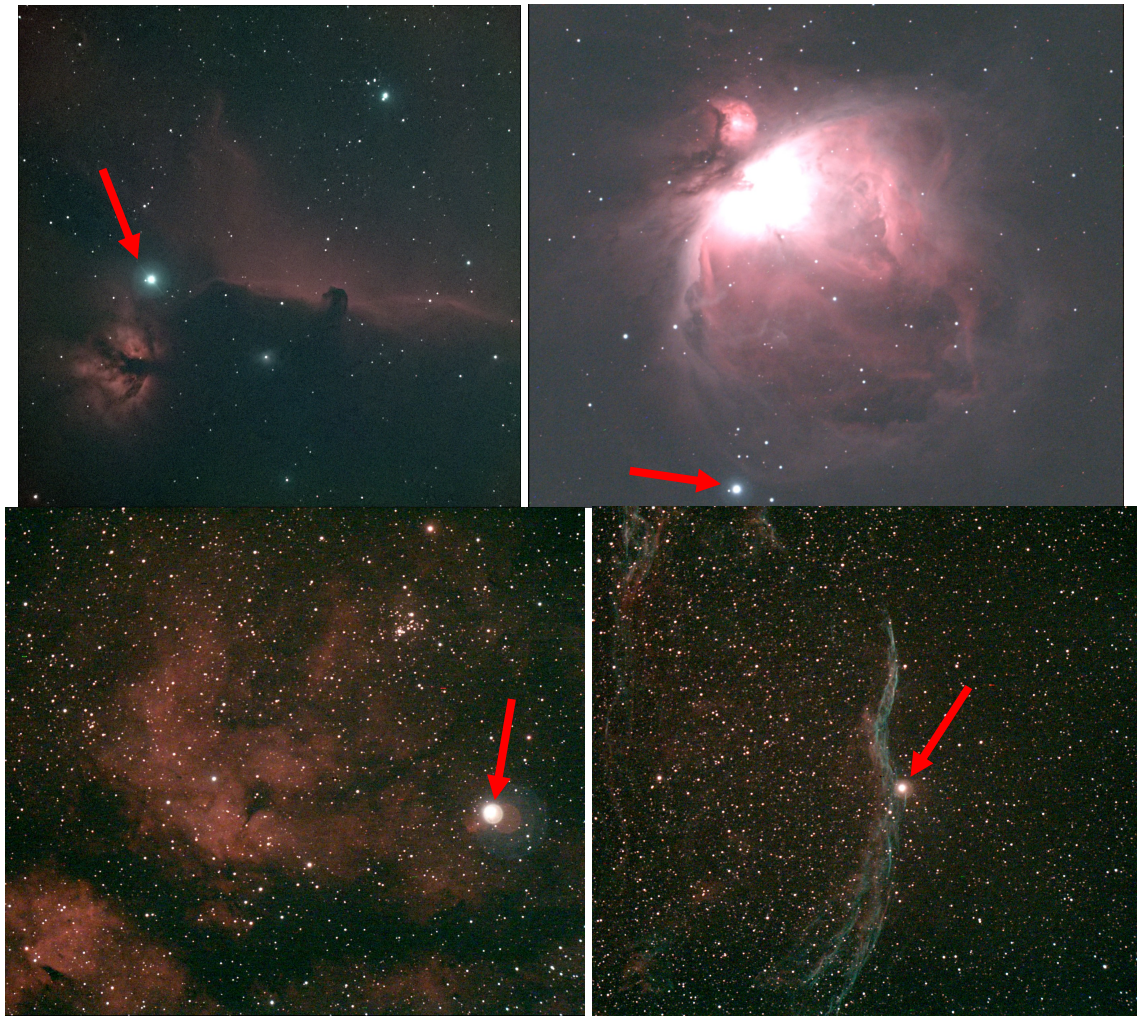

Figure 3 Sample Images with Prominent Star Halos

Star	Nearby Object	Mag	Colour Index (B-V)	Surface T	Filter Type when Halo Captured
α-Lyrae (Vega)	-	+0.00	0.00	9600K	all types
ζ -Orionis (Altnitak)	Flame, Horsehead	+1.85	-0.11	29,000K	multi-narrowband
β-Persei (Algol)	-	+2.05	-0.05	13,000K	all types
γ-Cygni (Sadr)	IC1318	+2.20	0.67	5800K	multi-narrowband
ι-Orionis (Hatysa)	M42	+2.75	-0.22	32,500K	multi-narrowband
52-Cygni	Western Veil	+4.20	1.05	4700K	multi-narrowband
57-Cygni	Pelican	+4.80	-0.13	17,200K	multi-narrowband
56-Cygni	Pelican	+5.05	0.19	8100K	multi-narrowband
φ -Aurigae	Spider	+5.05	1.41	4000K	narrowband H-α
7-Sagittarii	M8	+5.35	0.51	6800K	narrowband O-III, narrow broadband
SAO 50298 (Cygnus)	North American	+5.55	0.98	4800K	multi-narrowband
SAO 186135 (Sagittarius)	M20	+5.70	-0.03	11,600K	narrow broadband
SAO 186247 (Sagittarius)	M8	+6.85	0.07	9100K	narrow broadband
TYC 6842-1110-1 (Sagittarius)	M8	+10.25	1.48	4000K	narrowband O-III
TYC 6842-1205-1 (Sagittarius)	M8	+10.10	1.70	3800K	narrowband O-III

Table 1 Summary of Star Properties from Sample Images Containing Halos

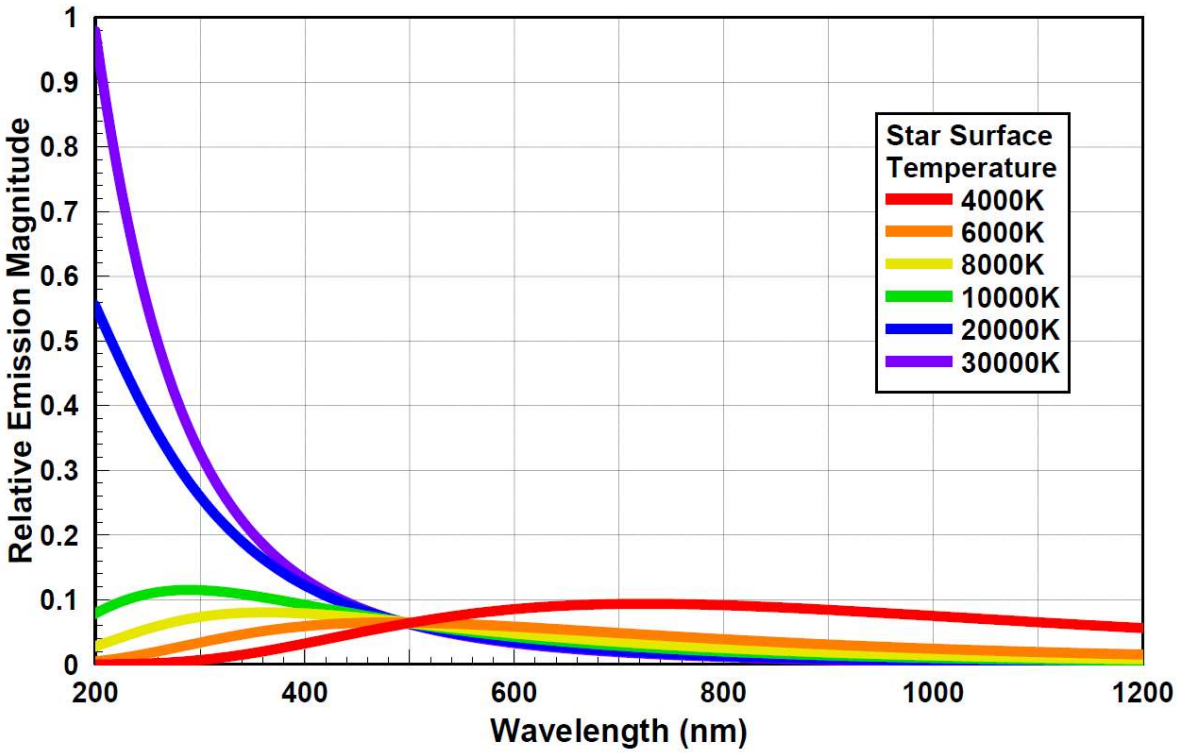

Figure 4 Comparison of Star Emission Spectrums – Stars w/ Equal Visual Brightness

3.0 Impact of Filter Position & Focal Ratio

The next investigation I performed was an experiment to determine how the appearance of a star halo changes with the position of the filter relative to the camera, or with the focal ratio of the optical setup. This experiment was performed by placing a filter known to cause halos at different distances from the sensor and recording images of the resulting halo. Focal ratio was varied in a separate test by varying the spacing between focal reducer and camera sensor, with the filter on the scope side of the focal reducer. Halo size, in pixels, was measured from the images as the primary output of the experiment.

3.1 Test Setup

The test setup consisted of a William Optics FLT98 refractor on a computerized equatorial mount. Images were collected using a ZWO ASI533MC Pro camera with IDAS NB-1 filter attached. The focal reducer used was an Astrophysics brand 0.67x in 2" format. The target star for the experiment was Arcturus (Mag= -0.04, Surface T=4290K). Varied spacing was achieve by using 'T' and 2" extension rings of various lengths. All data was collected in one evening (April 20th, 2022) from my backyard in central Ottawa, Canada.

3.2 Results

Figure 5 summarizes the results of my test. When the filter was placed alone on the scope, the distance between the filter and the sensor made no significant difference in the size of the halo. This observation is consistent with the assertion made in Section 1.1, and confirms that the halo is

most likely due to intra-filter reflections. When the focal reducer alone was used, a halo was observed that grew in size with the distance between focal reducer and sensor. This halo was presumably due to a reflection between the focal reducer and the camera sensor. When the filter was placed on the telescope side of the focal reducer, and the focal reducer distance varied relative to the sensor, the resulting halo size got smaller with increasing distance (i.e. decreasing focal ratio). Not performed was a test with the filter between the focal reducer and the sensor. Past experience has shown that such a configuration can result in numerous halos and ghosts simultaneously.

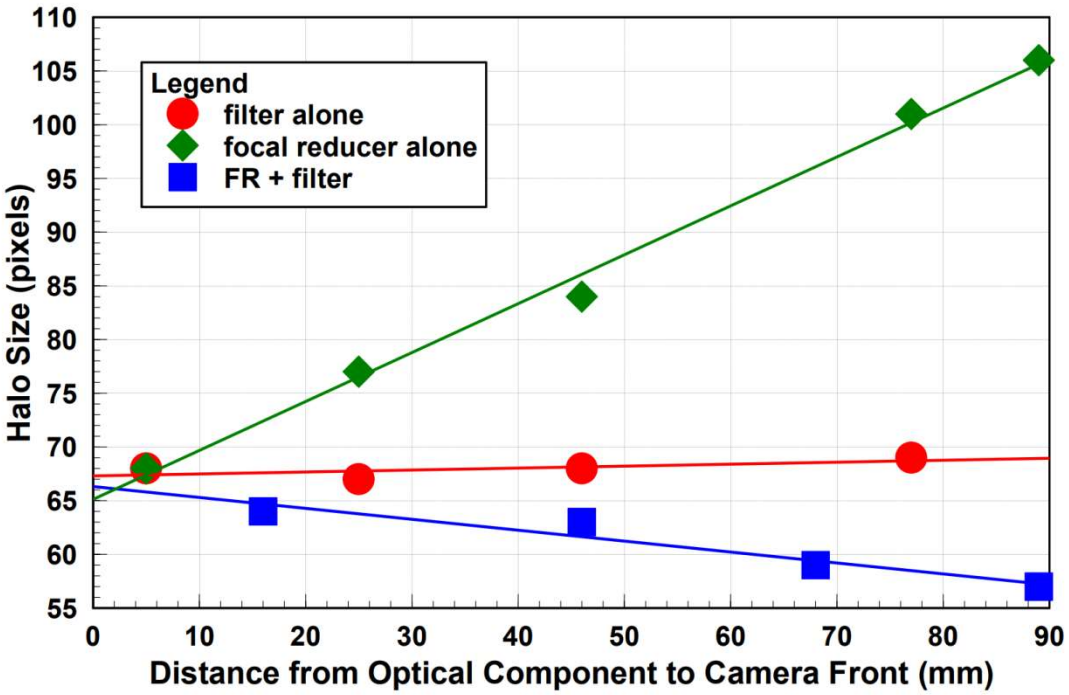

Figure 5 Results of Filter Spacing/Focal Ratio Test

4.0 Comprehensive Imaging Survey of Filter Halos

There is a large amount of anecdotal evidence available online regarding the prevalence of halos when using particular filters. I was not however able to find any prior test results involving more than one or two filters. My researching of filters over the past ten years has resulted in my accumulating a large variety of filters, offering an opportunity to perform a reasonably comprehensive survey of filters to determine their propensity for generating halos.

4.1 Test Setup

This experiment was performed using a Willam Optics FLT98 refractor at its native f-ratio of f/6.3, mounted on a computerized equatorial mount. Image data was collected using a ZWO ASI533MC Pro camera with ZWO 2" filter drawer attached. Data was collected on two separate occasions: September 29th, and October 22nd, 2022. The target star for the first session was Vega (Mag= +0.00, Surface T=9600K), and for the second session Algol (Mag= +2.05, Surface

T=13,000K). A total of 45 different filters were tested, the list of which is provided below in Table 2. Due to time constraints, only 16 of the 45 filters were tested during the first session. All data was collected from my backyard in central Ottawa, Canada.

#	Brand & Model	Type	%LT	#	Brand & Model	Type	%LT	#	Brand & Model	Type	%LT
1	Antlia ALP-T	multi-narrowband	2.3	16	IDAS LPS-P2	multiband	40.5	31	Optolong 3.0nm SII	narrowband	0.6
2	Arcturus UHC	medium broadband	37.4	17	IDAS LPS-P3	multiband	41.2	32	Optolong 6.5nm SII	narrowband	1.5
3	Askar 3nm Dual Band	multi-narrowband	1.9	18	IDAS NB-1	multi-narrowband	12.5	33	Optolong 7.0nm Halpha	narrowband	1.2
4	Astronomik Hbeta visual	narrowband	13.0	19	IDAS NB-2	multi-narrowband	16.1	34	Optolong CLS	wide broadband	38.2
5	Astronomik IR Cut	UV/IR cut	65.2	20	IDAS NB-3	multi-narrowband	15.3	35	Optolong IR Cut	UV/IR cut	66.9
6	Astronomik OIII visual	narrowband	13.9	21	IDAS NBZ	multi-narrowband	6.1	36	Optolong L-eNhance	multi-narrowband	8.9
7	Astronomik ProPlanet 642	IR pass	27.8	22	Lumicon Deepsky	wide broadband	38.5	37	Optolong L-eXtreme	multi-narrowband	3.2
8	Astronomik UHC	medium broadband	36.0	23	Meade Broadband	wide broadband	45.1	38	Optolong L-Pro	multiband	36.7
9	Baader IR Pass	IR pass	28.2	24	Meade OIII	narrow broadband	30.3	39	Optolong L-uLtimate	multi-narrowband	1.5
10	Baader UHC-S	wide broadband	21.8	25	Omega 650BP10	narrowband	2.3	40	Optolong Nightsky Halpha	IR pass	38.0
11	Baader UV/IR Cut	UV/IR cut	62.0	26	Omega BDRB	UV/IR cut	44.2	41	Optolong UHC	medium broadband	34.5
12	IDAS 6.0nm OIII	narrowband	1.7	27	Omega NPB DGM Improved	multi-narrowband	8.7	42	Radian Triad	multi-narrowband	6.0
13	IDAS 6.8nm Halpha	narrowband	1.5	28	Omega XMV660/40	narrowband	9.1	43	Radian Triad Ultra	multi-narrowband	3.9
14	IDAS EAO1	wide broadband	20.0	29	Optolong 3.0nm Halpha	narrowband	0.6	44	STC Duo-Narrowband	multi-narrowband	6.9
15	IDAS LPS-D2	multiband	33.3	30	Optolong 3.0nm OIII	narrowband	0.8	45	ZWO Duo-band	multi-narrowband	11.9

Table 2 List of Filters Under Test

4.2 Results

A 60 second live stacked image of the target star was captured using each filter. The sub-exposure time was set according to the luminous transmissivity (%LT) of each filter, the objective of which was to collect images with the same overall exposure level. The resulting image captures, close cropped on the target star, are presented in Figures 6 through 9. The filter numbers referred to in the figures correspond to those in Table 2. Note that the images are presented in the order they were tested, not the order in Table 2, as some filters were of a higher priority to get tested than others and so were moved to the top of the testing order. Filters were prioritized because of the length of time required to perform the testing. A batch of 15 filters required approximately 1 hour to collect image data.


No Filter Filter 01 Filter 08 Filter 11


Filter 17 Filter 15 Filter 18 Filter 21


Filter 22 Filter 36 Filter 37 Filter 39


Filter 33 Filter 30 Filter 43 Filter 45


Filter 27

Figure 6 Image Captures from 1st Session – Vega (9600K)

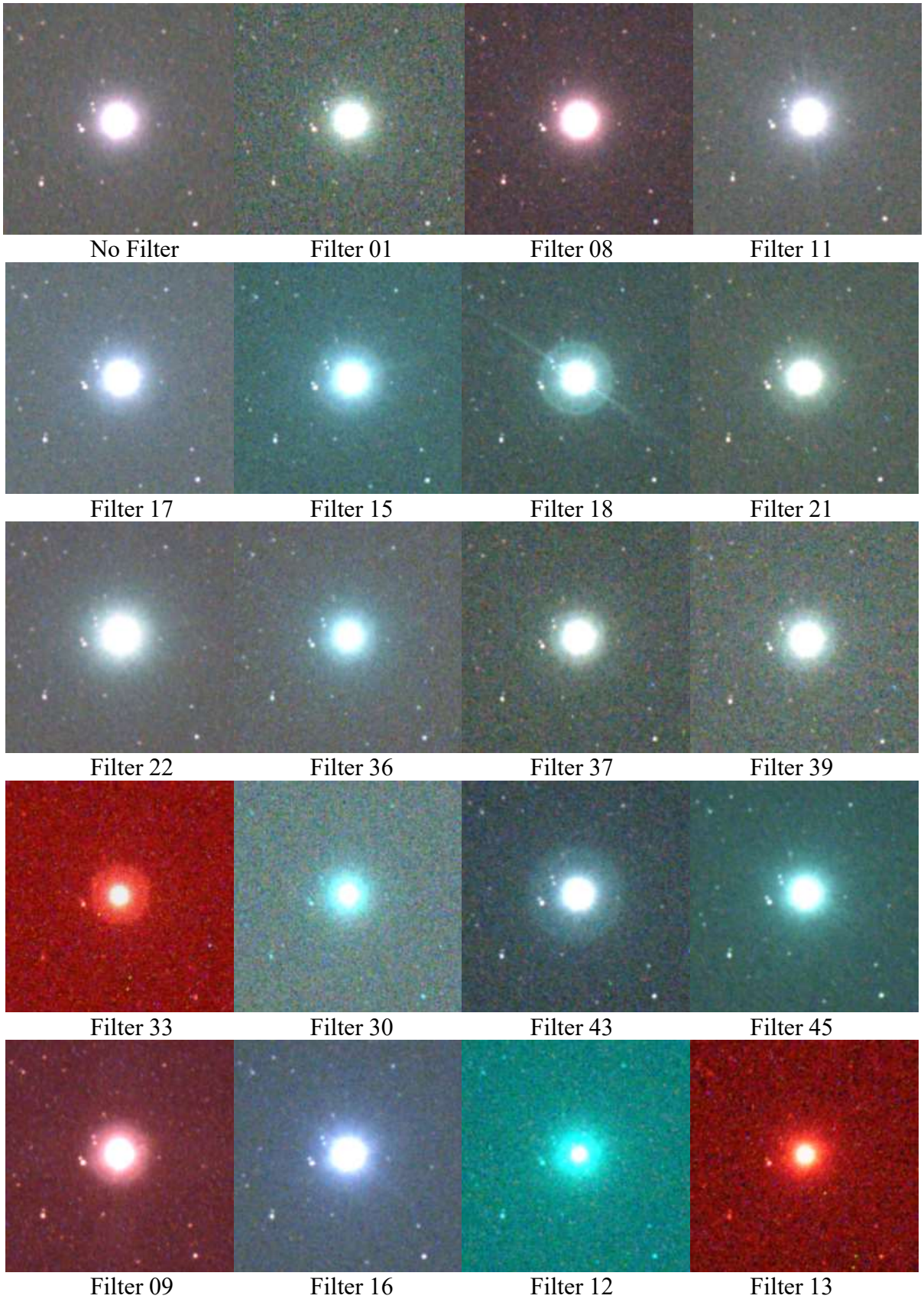

Figure 7 Image Captures from 2nd Session, Part 1 – Algol (13,000K)

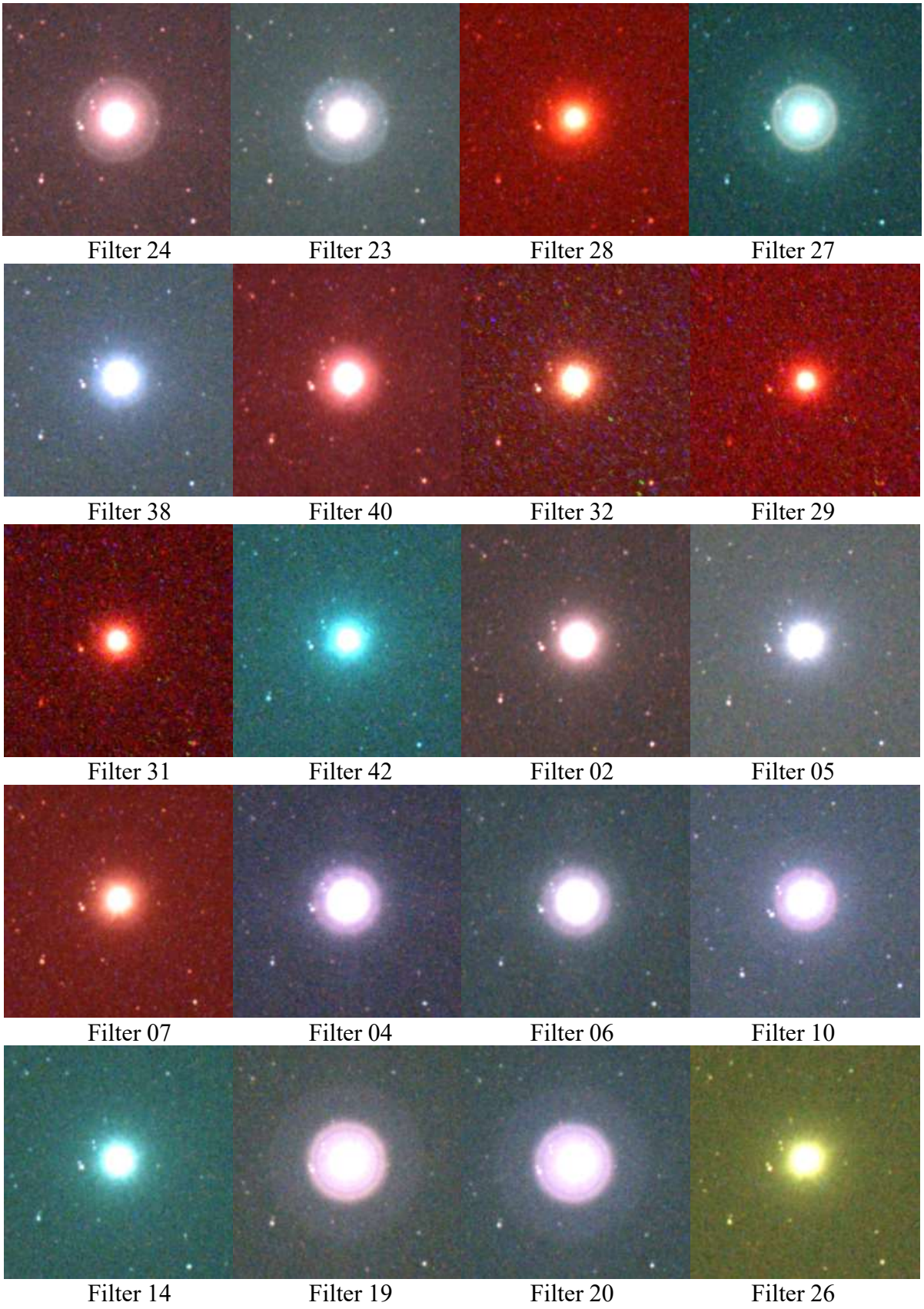

Figure 8 Image Captures from 2nd Session, Part 2 – Algol (13,000K)

Figure 9 Image Captures from 2nd Session, Part 3 – Algol (13,000K)

The star test revealed a wide range of halo severities, from filters with bright triple halos down to filters with no discernable halo at all. Halo sizes varied, but in a way that was consistent with the manufacturer stated filter glass thickness; thicker glass produced larger halos. To enable a more quantitative comparison between filters, each image was analysed in AstroImageJ to extract the contrast between halo and background in each colour channel. These values are plotted in Figure 10 relative to the "no filter" case. A positive relative contrast value means that the area around the star was found to be brighter than the no filter case by the noted factor, and a negative value means the area around the star was darker than the no filter case. Thus, a larger positive number indicates a stronger, more intrusive halo. The halo contrast values are presented in Figure 10 as a sum of the three individual colour channel values for each filter. The length of each bar sub-component (red, green, blue) illustrates the relative contribution of the halo in each colour channel to the overall halo strength for that filter. Overall halo relative contrast values of 1.0 or less can be interpreted as the filter was found to not have a significant halo. An overall relative contrast value greater than 3.0 indicates a filter with a very bright and intrusive halo. The green colour channel was found to be the one making the largest contribution to overall halo contrast for most filters. There were however a fair number of filters with blue channel dominated halos as well.

With a quantitative measurement of each filter's halo brightness in hand, the next step was to measure the physical properties of each filter with the hopes of finding a property that correlated with the halo data, to find the root cause for the halo. The first property investigated was reflectivity, as discussed in the next section.

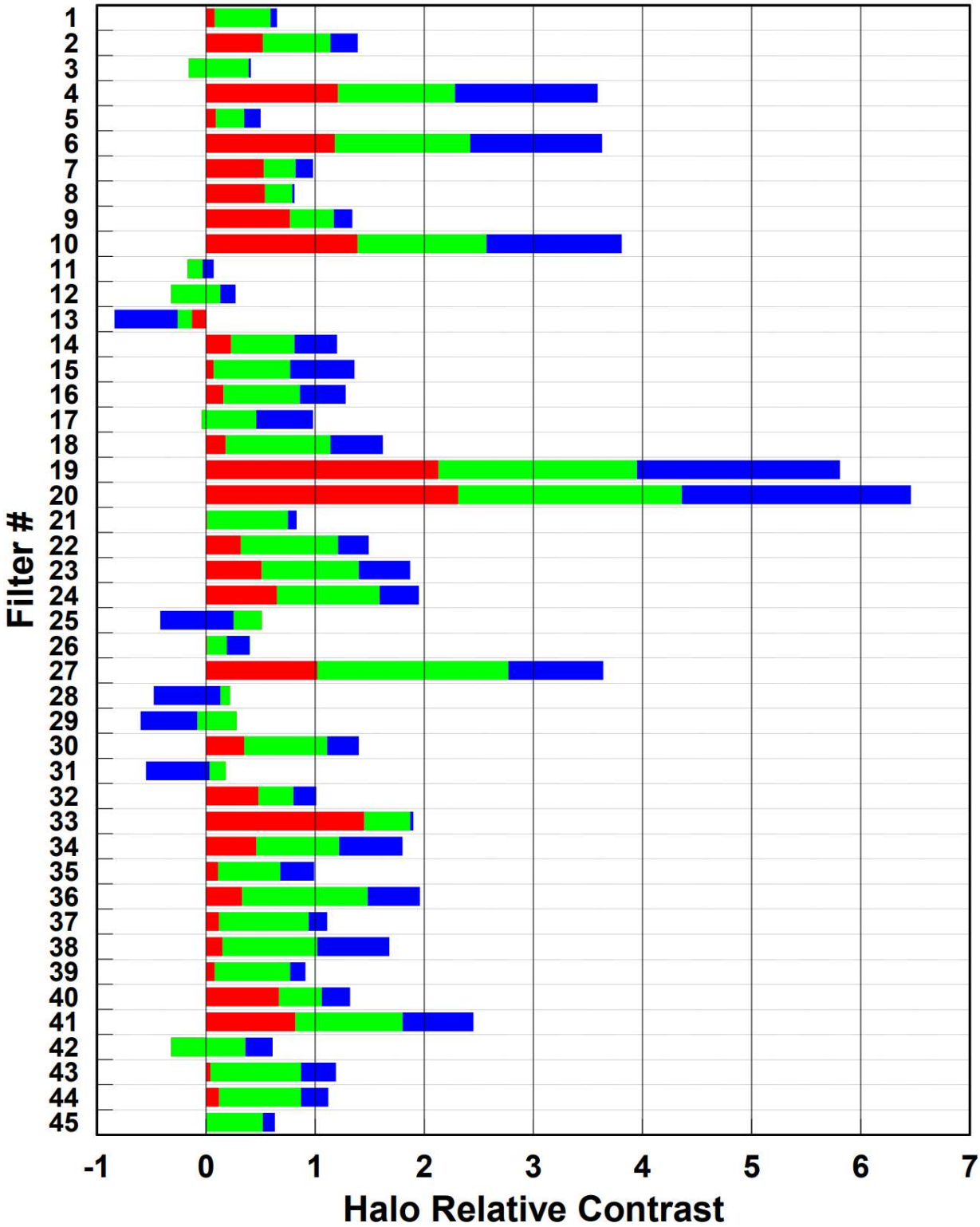

Figure 10 Measured Halo Relative Contrast

5.0 Filter Reflectivity

When I started this project, the easily accessible reference material I found online gave me the impression that halos are primarily caused by reflections between the filter and the camera sensor window. I have since come to understand that is not the case, but at the time this impression led me in the direction of measuring filter spectral reflectivity. The results of this avenue of investigation are summarized in this rest of this section.

5.1 Test Setup

To be able to measure the spectral reflectivity of a filter required me to construct a rudimentary reflectometer. This is a fairly simple instrument consisting of a collimated light source pointed at the filter at a fixed angle, and a sensor positioned over the filter at an appropriate location to receive the light that has been reflected off of it. In my case I used a 4700K 12VDC halogen spot bulb jerry-rigged to the eyepiece end of Meade 50mm finder scope as my collimated light source. The reflected light was gathered by a collimating lens attached to the end of a fibre optic cable, with an Ocean Insight USB4000 spectrometer on the other end. A photo of the apparatus I constructed is shown in Figure 11. I constructed the back plate to allow for two different test angles: 60°, and 20° off axis from the filter. I also added a diffusing filter on the end of the finder scope (a piece of plastic grocery bag, not shown in Figure 11) to provide a more uniform light source. The final component of the setup was a reflection reference. I did not have a calibrated reference, so instead I used an aluminized 1st surface mirror as my reference. As a result all my reflectivity measurements are relative to this aluminized mirror. An alternative view of my setup while in use is provided in Figure 12.

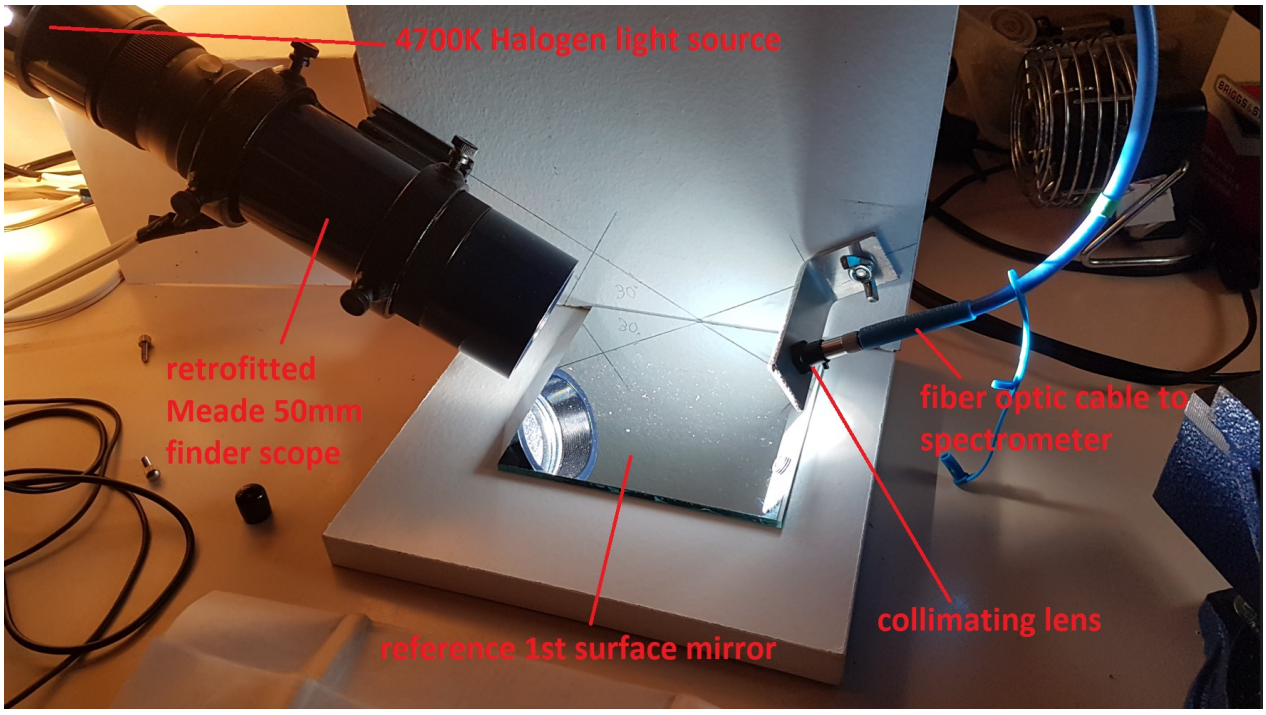

Figure 11 Home-built Reflectometer, 60° Configuration

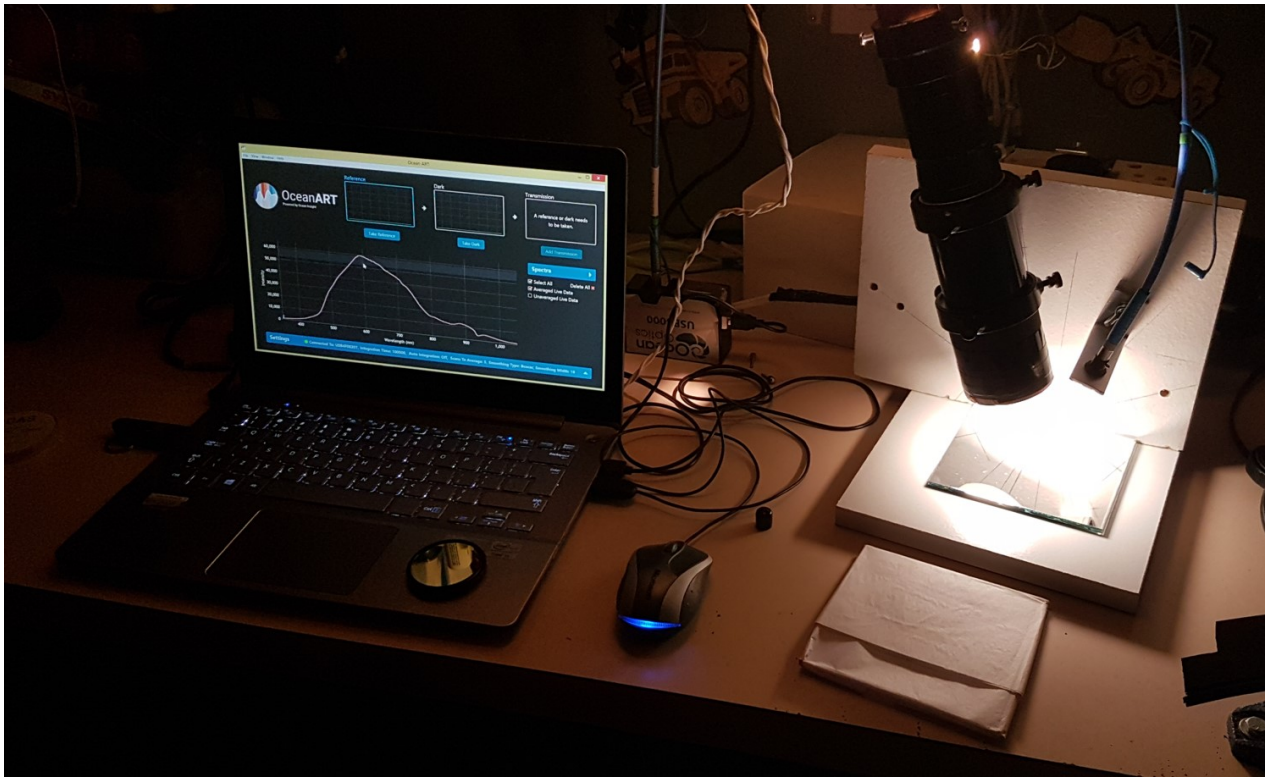

Figure 12 Reflectometer Apparatus in Use, 20° Configuration

A weakness of my apparatus was that the source light intensity at the UV and Near-IR ends of the spectrum was low, resulting in a large error in my reflectivity measurements at those wavelengths. For my purposes I felt that this deficiency was acceptable as my objective was primarily to evaluate the rough order magnitude reflectivity of each filter; i.e. is the filter reflective or not.

5.2 Results

Figure 13 presents an example of the reflectivity data that was captured using the above described apparatus. The plot shown is for the measurement that was made of Filter #1, the Antlia ALP-T. The two 5nm wide pass bands of this filter are visible as low reflectivity spikes in the graph at ~490 and 650nm, the pass bands being shifted down in wavelength from the filter's specification due to the reflection being observed at 20° off axis and thus exhibiting some band shift. The side of the filter that faces the telescope (red line) is otherwise very reflective across the entire visible and near-IR spectrum. The side of the filter that faces the camera (blue line) was measured to have very similar reflectivity to the telescope facing side, except in the 400 to 470nm range. The filter shows clear evidence of an anti-reflective coating on this side, resulting in the reduced reflectivity measured at the blue end of the spectrum. A similar low reflectivity treatment in the blue part of the spectrum was measured on several other filters including: Askar 3nm Dual Narrowband, Lumicon Deepsky, Omega XMV660/40, all the Optolong SHO narrowband filters, and the Optolong L-uLtimate. The low reflectivity coating gives the filter a pronounced gold colour on the side that faces the camera. As will be shown later in this report, the presence of an

anti-reflective coating on the camera facing side of the filter can help to reduce halos. Similar plots of measured spectral reflectivity for all the other tested filters can be found in Appendix A.

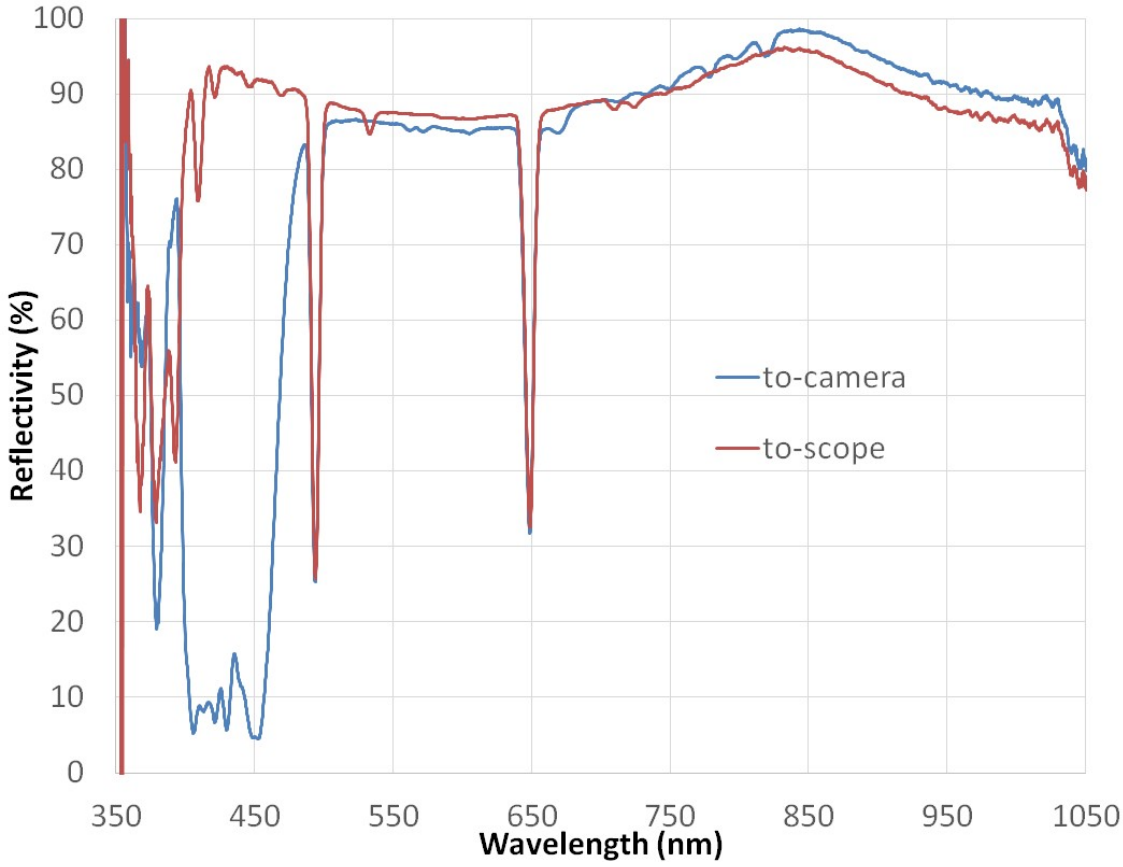

Figure 13 Example Filter Reflectivity Measurement, 20° Config, Filter #01

Average relative reflectivity has been calculated for each filter using the measured data. This has been done in three bands of interest: 400-450nm (blue), 500-600nm (green/yellow), and 800-900nm (near-IR). These three bands correspond to parts of the spectrum that are typically not of interest to amateur astronomers and tend to contain light pollution. A low reflectivity value in one of these bands would indicate the presence of either high filter transmissivity or an anti-reflective coating in that band. The results have been summarized in Figure 14. The reflectivity in each of the three bands has been plotted stacked one next to the other so that an overall impression of filter reflectivity can be visualized from the plot.

Collecting the reflectivity data and reducing it was a labour intensive process. I was therefore quite disappointed when there turned out to be very little correlation between my measured halo contrast data and my reflectivity data. Although some filters with no visible halo had low reflectivity, others had very high reflectivity. Based on these results it was clear to me that I was not seeing the whole picture and that more research was required, as will be discussed in more detail in the next section.

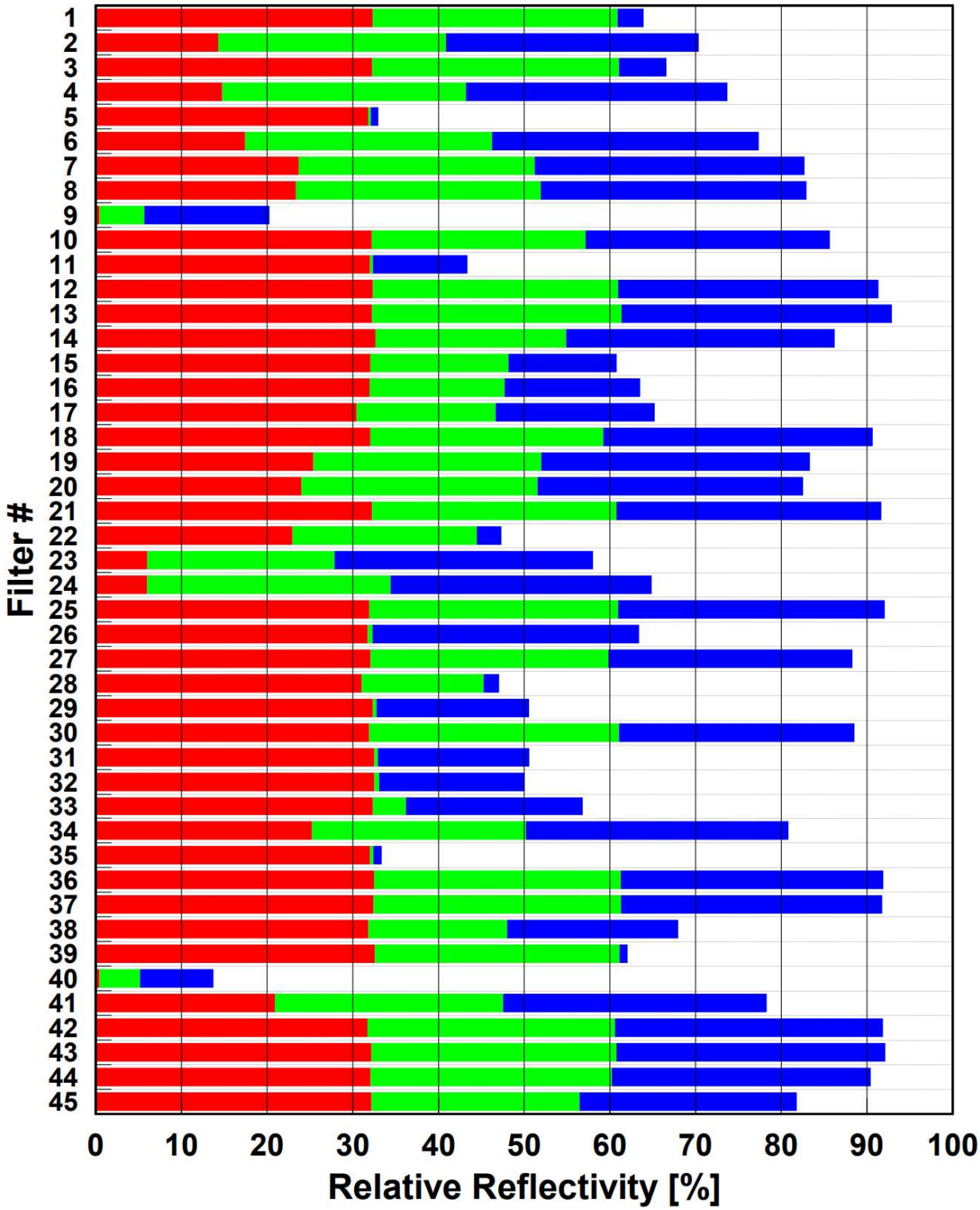

Figure 14 Measured Filter Relative Reflectivity

6.0 Filter Off-Band Blocking

When I found that camera-side reflectivity did not strongly indicate as the cause of halos I went back to the manufacturer provided data to see if there was some other physical parameter that might be responsible. I noticed that the off-band blocking reported by the manufacturers did correlate to some extent with my halo data. Table 3 summarizes the manufacturer provided data that I based my observation on. From this small sampling of filters, it seemed that off-band blocking might be a significant factor in halo generation. To be sure I needed to measure this property from my collection of sample filters.

Filter	OEM Quoted Off-Band Blocking		Measured Halo Contrast		
	Transmission	OD	Red	Green	Blue
Optolong L-eNhance	< 1%	> OD2	0.33	1.15	0.48
IDAS NBZ	< 0.1%	> OD3	0.01	0.74	0.08
Optolong L-uLtimate	< 0.01%	> OD4	0.08	0.69	0.14
Antlia ALP-T	< 0.003%	> OD4.5	0.08	0.51	0.06
Askar 3nm Dual Narrowband	< 0.001%	> OD5	-0.16	0.57	-0.02

Table 3 Filter Manufacturer Quoted Blocking vs. Measured Halo

Before describing my measurement process it is important to first provide a clear definition of what "off-band blocking" means. The purpose of a filter is to pass light from objects we want to observe while blocking as much unwanted light as possible. Wavelengths of light the filter is designed to pass are considered to be "in-band", and wavelengths the filter is designed to block are "off-band". Reducing the transmissivity of a filter to off-band wavelengths is desirable for good filter performance, but it comes at a cost as more interference layers are required to achieve this result. As a result, the extent of off-band blocking that is provided by different filter manufacturers varies widely and is correlated closely with filter price. The common way of expressing the magnitude of off-band blocking is to use the property called Optical Density (OD). OD is related to transmissivity by the following equation:

$$OD = - LOG_{10}(transmissivity)$$

, where transmissivity is expressed as a fraction not as a percentage. The measurements I made of filter OD is what is discussed in the remainder of this section.

6.1 Test Setup

To be able to measure OD required me to come up with an apparatus capable of high sensitivity and accuracy. My past filter transmissivity measurements have been made to within +/- 1%, but to measure blocking I would need accuracy three orders of magnitude better, an accuracy of +/- 0.001%. To achieve this level of accuracy required me to use my spectrometer with a variable exposure time. The reference light intensity was measured with no filter in place at a short exposure time, on the order of 0.1ms. When the filter was added, the exposure time would be increased as required to get a light intensity reading that was well above the instrument noise

level. Noting both the exposure time and the light intensity reading allowed me to calculate the resulting OD. The maximum practical exposure time used was 10,000ms (10sec), giving me sufficient instrument sensitivity to measure filter blocking down to OD 5. The collimated halogen light source from my reflectometer apparatus was reused for this measurement setup. Between the light source and the filter under test was placed a band pass filter that allowed me to work with a limited part of the spectrum at one time. This was necessary to keep the spectrometer's CCD sensor from saturating and giving erroneous results. The list of filters used is listed below. A photo of the test apparatus is provided in Figure 15.

- 400 to 450nm band: Hoya B390 band pass filter
- 550nm band: Baader Planetarium Solar Continuum filter
- 800 to 900nm band: generic 680nm high pass filter

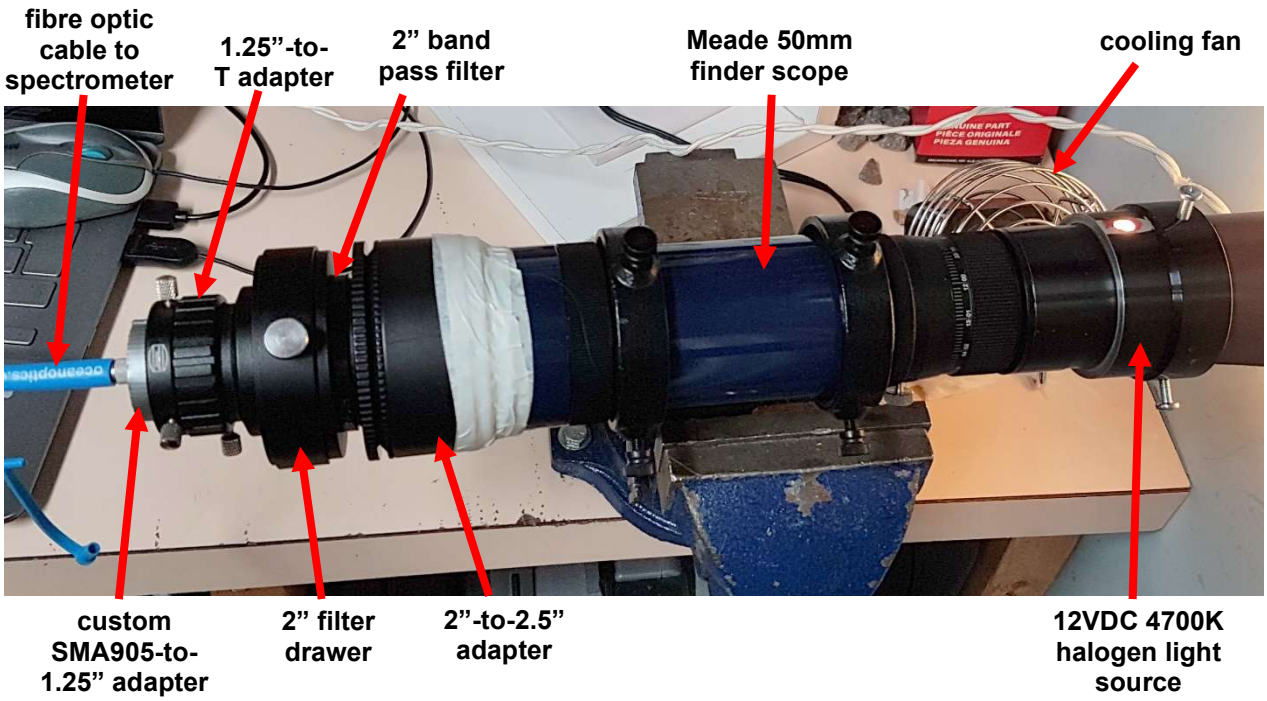

Figure 15 Home Built Off-Band Blocking Measurement Apparatus

To keep the sensitivity of my test apparatus high enough to measure large OD values required me to use my spectrometer with the largest entrance slit size, i.e. let in as much light as possible. The spectrometer used was an Ocean Insight USB4000 with no entrance slit, the entrance size being determined by the diameter of optical cable I was using which in this case was 1.5mm. As a result of having such a large entrance slit, the accuracy of my spectrometer readings around steep changes in transmissivity was very poor. This fact limited me to measuring blocking at wavelengths that were well away from the typical filter pass bands: 400-450nm, 530nm, and 800-900nm.

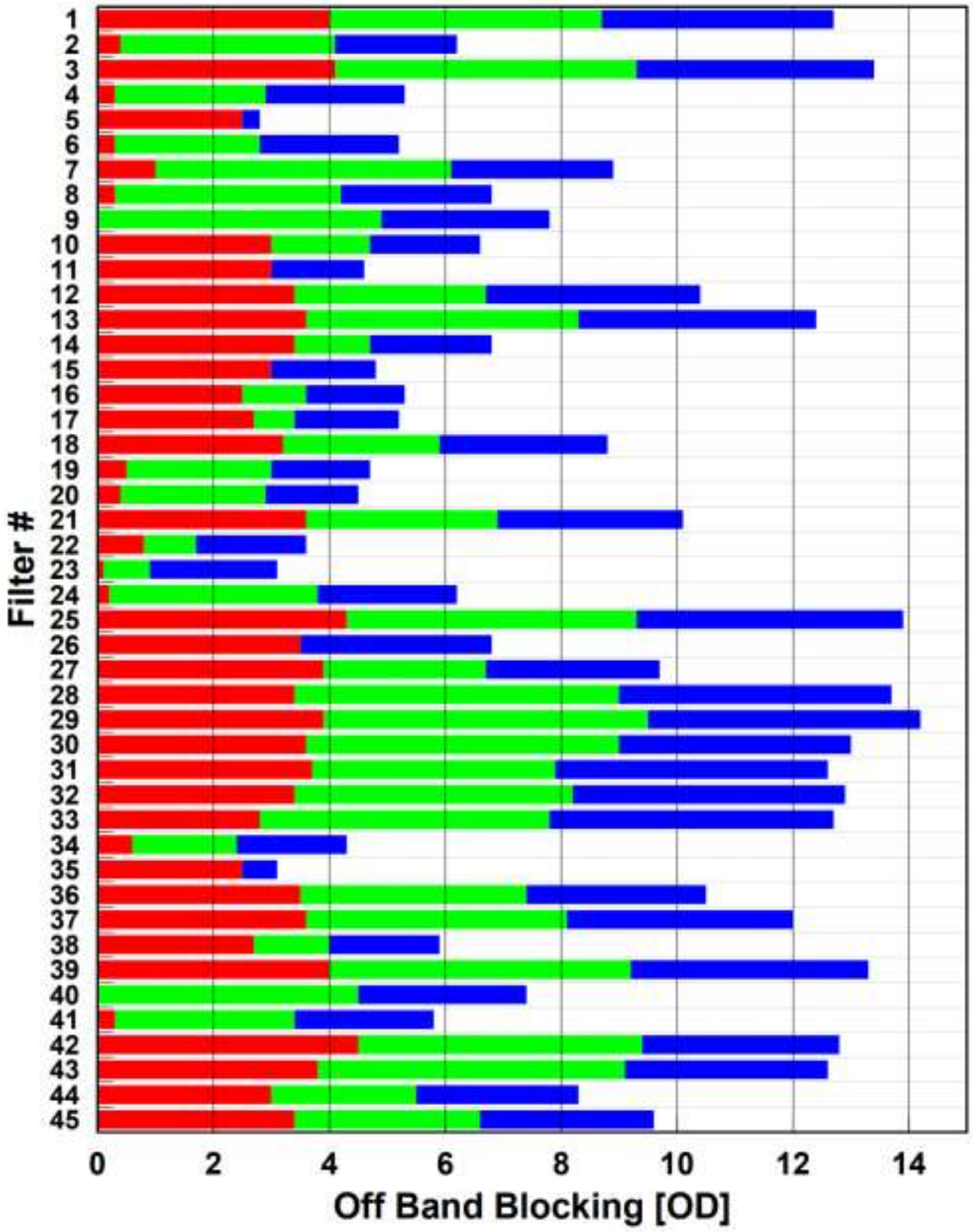

Figure 16 Measured Filter Off-Band Blocking

6.2 Results

The blocking in each of the three bands listed above was measured using my apparatus for all 45 filters in my list. It was a labour-intensive activity, taking just under eight hours to complete. The results are plotted in Figure 16. As with the previous comparison plots, the measured OD in each band is shown stacked together to give an overall impression of how good the blocking is of one filter compared to another. I was surprised to find such a large variation in blocking, some filters having blocking less than OD2 in each band while others were over OD5. In general, filters with low blocking values were either lower priced filters or filters intended for visual use only. Comparing my off-band blocking results to my halo contrast results, it is evident that there is some level of correlation present. The extent of this correlation is discussed in the next section.

7.0 Correlation of Filter Properties

My approach to the problem of "what causes halos" has essentially been to measure a number of filter physical properties and look to see if any of them correlated with the presence of halos in my images. I have generated a large amount of data through the course of the testing described above, so coming up with an efficient way of visualizing it was important. The data presentation I settled on is shown in Figures 17 to 19. The graphs plot the measured off-band blocking versus relative reflectivity in each of the three colour channels. Each data marker is coloured based on the measured halo contrast value for that filter, with black representing no visible halo and pink representing a very bright halo. The number in yellow text inside each data marker is the filter number corresponding to that data point. I have added a ring around data markers corresponding to IR pass, H-α, and S-II filters as they seem to have a different behavior than the other filters. Similarly, I have added a box around all the UV/IR cut filter data points which also behave differently than the other filters.

In general, the data suggests that filters with high levels of off-band blocking, OD values >4, have little or no discernable halos. Filters with off-band blocking less than OD4 may or may not present significant halos, there is too much scatter in the data below OD4 to make a more definitive observation. Filters having the brightest halos tended to have both low off-band blocking and high reflectivity. Filters with moderate reflectivity, in the 30-60% range, have generally less halo contrast than filters with higher reflectivity, even when their off-band blocking is low. There are several filters that defy these basic observations, having no discernable halos but also having low off-band blocking and high reflectivity. I do not have a good explanation for these outliers except that they may be due to uncertainty in my measurements, especially in regards to the evaluation of halo contrast. Figures 17 to 19 are based on the data from my 2nd imaging session which used a 13,000K star as the target. Redoing the test multiple times using stars of varying temperature and magnitude may be required to resolve my issue with outliers and scatter. For the purposes of this report, I am content with the results, and have no intention of collection additional data.

All of the data plotted in Figures 17 to 19, including my measurements of filter reflectivity, off-band blocking, and halo contrast, has been tabulated for easy reference. The summary table can be found in Appendix B.

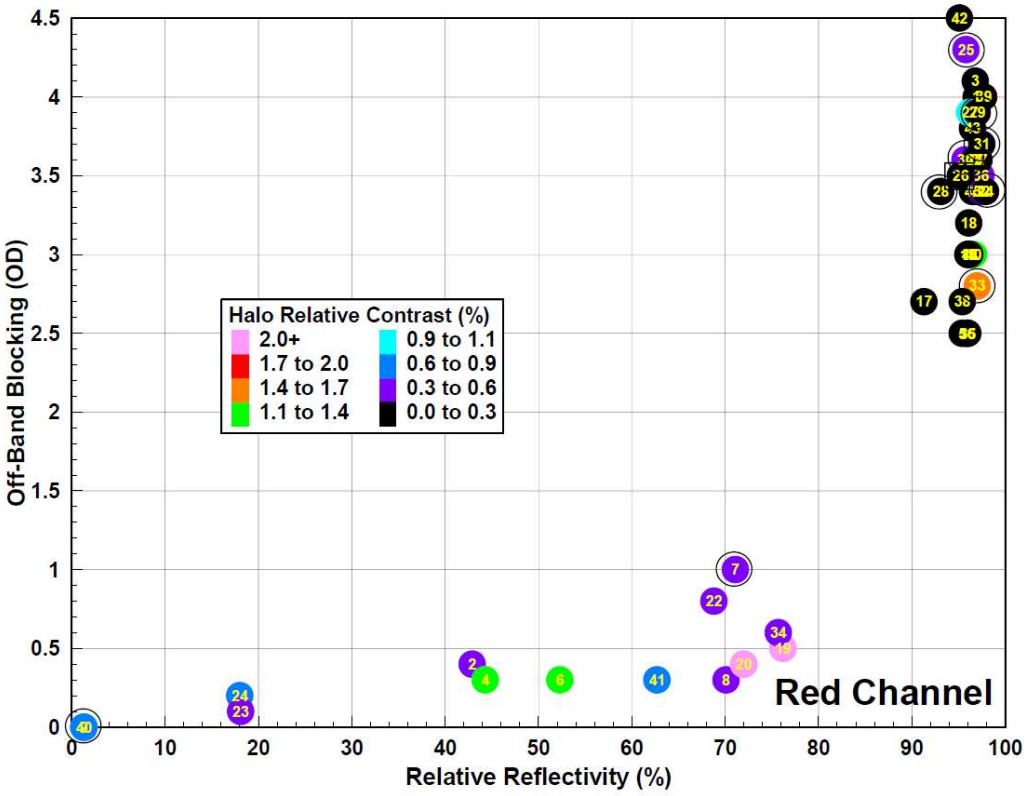

Figure 17 Filter Off-Band Blocking vs Relative Reflectivity, Red Channel

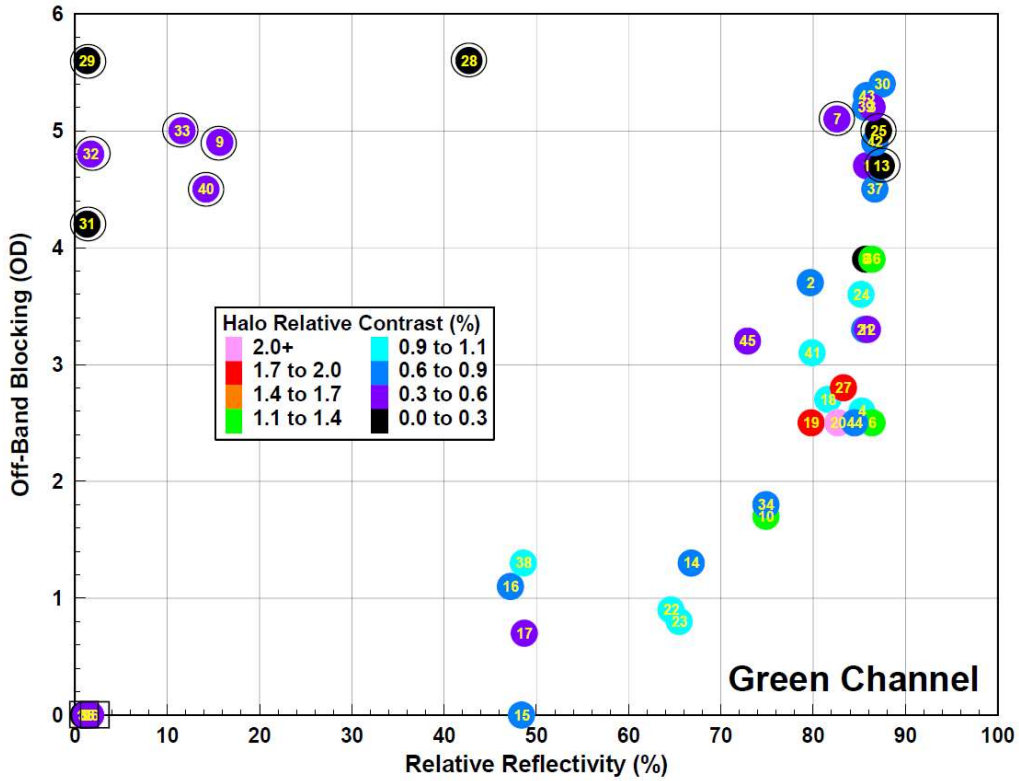

Figure 18 Filter Off-Band Blocking vs Relative Reflectivity, Green Channel

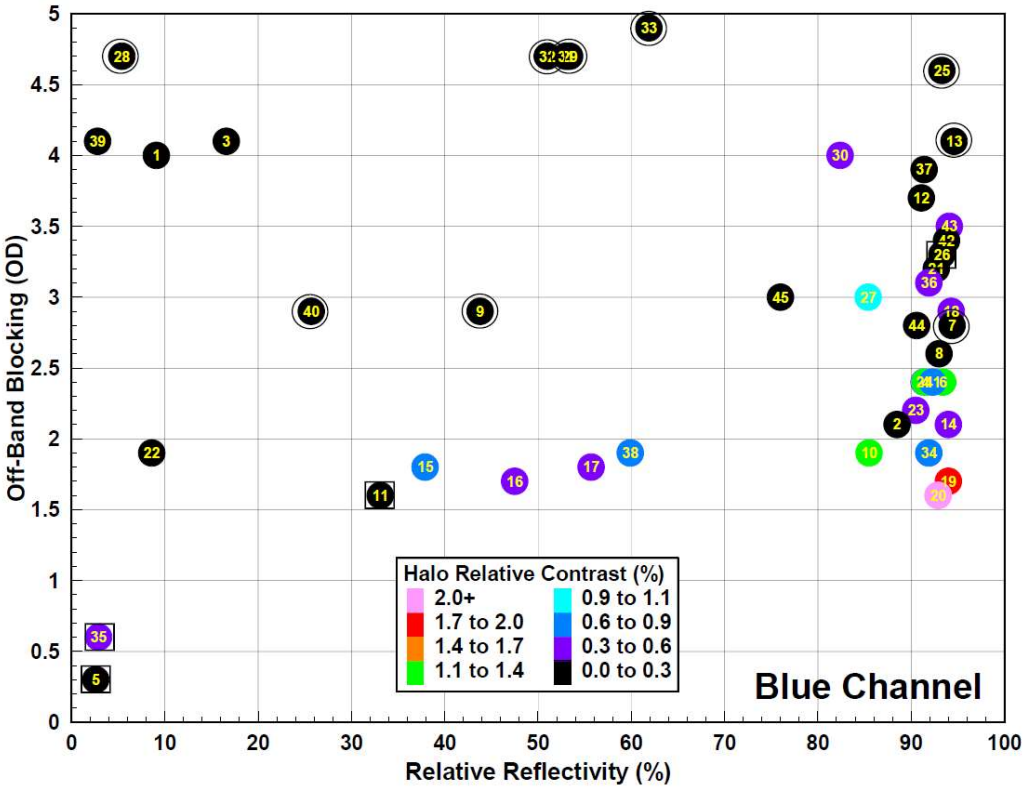

Figure 19 Filter Off-Band Blocking vs Relative Reflectivity, Blue Channel

8.0 Halo Generation Simulation

Each of the individual experiments summarized in the preceding sections has led to an important observation regarding the behavior of filter related star halos. In my opinion the main observations to come from my testing have been:

1. The severity of halos is related to star temperature, with hot stars being more prone to halos than cool stars;
2. Halos are caused primarily by intra-filter reflections, but filter-camera reflections can also contribute to the problem;
3. A filter's tendency to produce halos is strongly dependant on the filter's off-band blocking, with low blocking being more prone to halos than high blocking; and
4. A filter's tendency to produce halos is somewhat dependant on the filter's reflectivity, with high reflectivity being more prone to halos than low reflectivity.

To confirm my observations analytically I have constructed a numerical simulation that predicts the brightness of the halo generated by a filter with known off-band blocking and reflectivity, for a range of star temperatures. The simulation assumes the filter properties of a typical multi-narrowband filter with 15nm wide pass bands. The transmissivity plot for the theoretical filter is shown in Figure 20. Off-band blocking is varied from OD1 to OD5 in the simulation. Four different variations of this theoretical filter are considered: Filter A has no anti-reflective coatings (%reflectivity = 100 – %transmissivity), Filter B has anti-reflective coatings treating just the blue

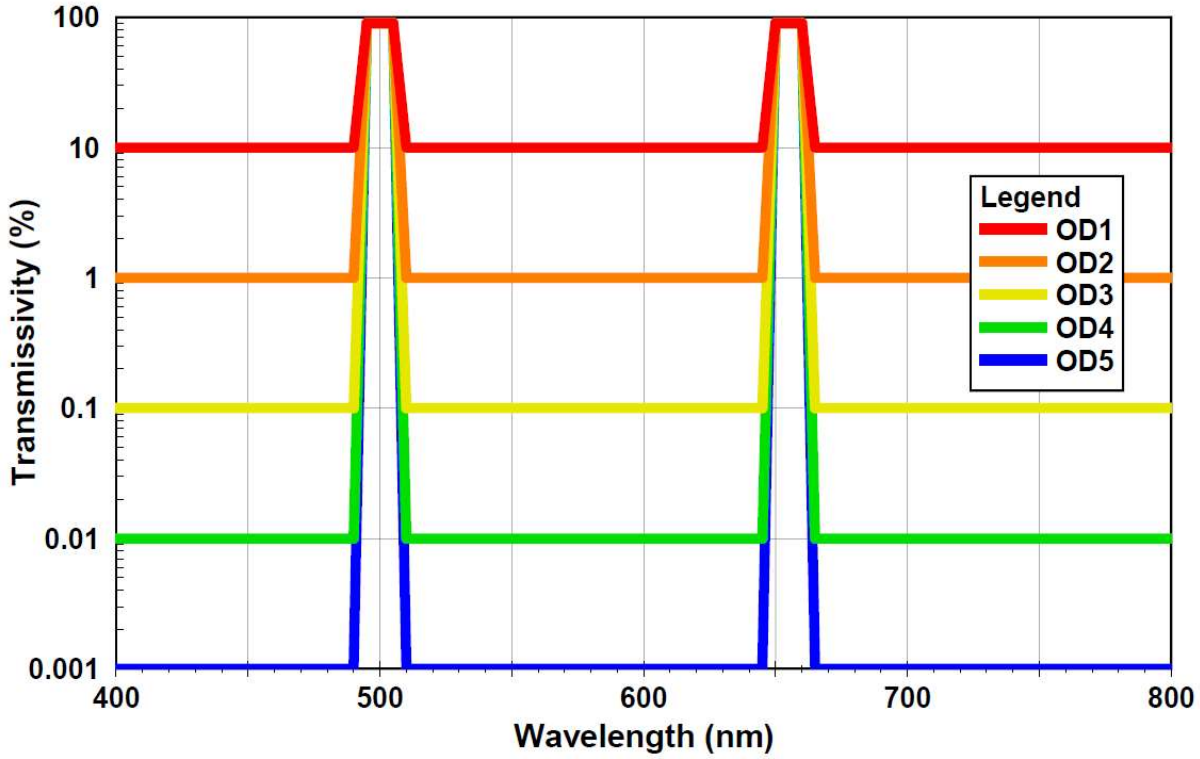

Figure 20 Theoretical Filter Used in Simulation

part of the spectrum (<480nm), Filter C has anti-reflective coatings treating the green part of the spectrum (520-630nm), and Filter D has anti-reflective coatings treating the red & infrared part of the spectrum (>680nm). The hypothetical sensor being used for the analysis is a monochrome back illuminated CMOS (IMX174). The same star emission spectrums presented in Figure 4 were used in the simulation. The simulated halo brightness is calculated by propagating the star's off-band emission through the filter, reflecting twice along the way to the sensor. The calculation is performed spectrally using a 5nm wavelength resolution.

The total off-band star emission getting to the camera in the form of a halo is summed up and compared in Figure 21. Consider first the plot in the upper left which is for the filter with no anti-reflective coatings applied. Observation #1, that star temperature has an impact on halo brightness, is born out by the simulation however the magnitude of the variation in halo brightness with star temperature is not as significant as I was expecting. In addition, besides the halo brightness going up for very hot stars, it is also predicted to go up for very cool stars as well. I had not originally anticipated this, but it is consistent with the halo observations summarized in Table 1. It may be that my original assumption about only hot stars being prone to halos is due to an observing bias: halos are observed when using filters to image nebulae in star forming regions, which tend to contain young stars that are in general both hot and bright.

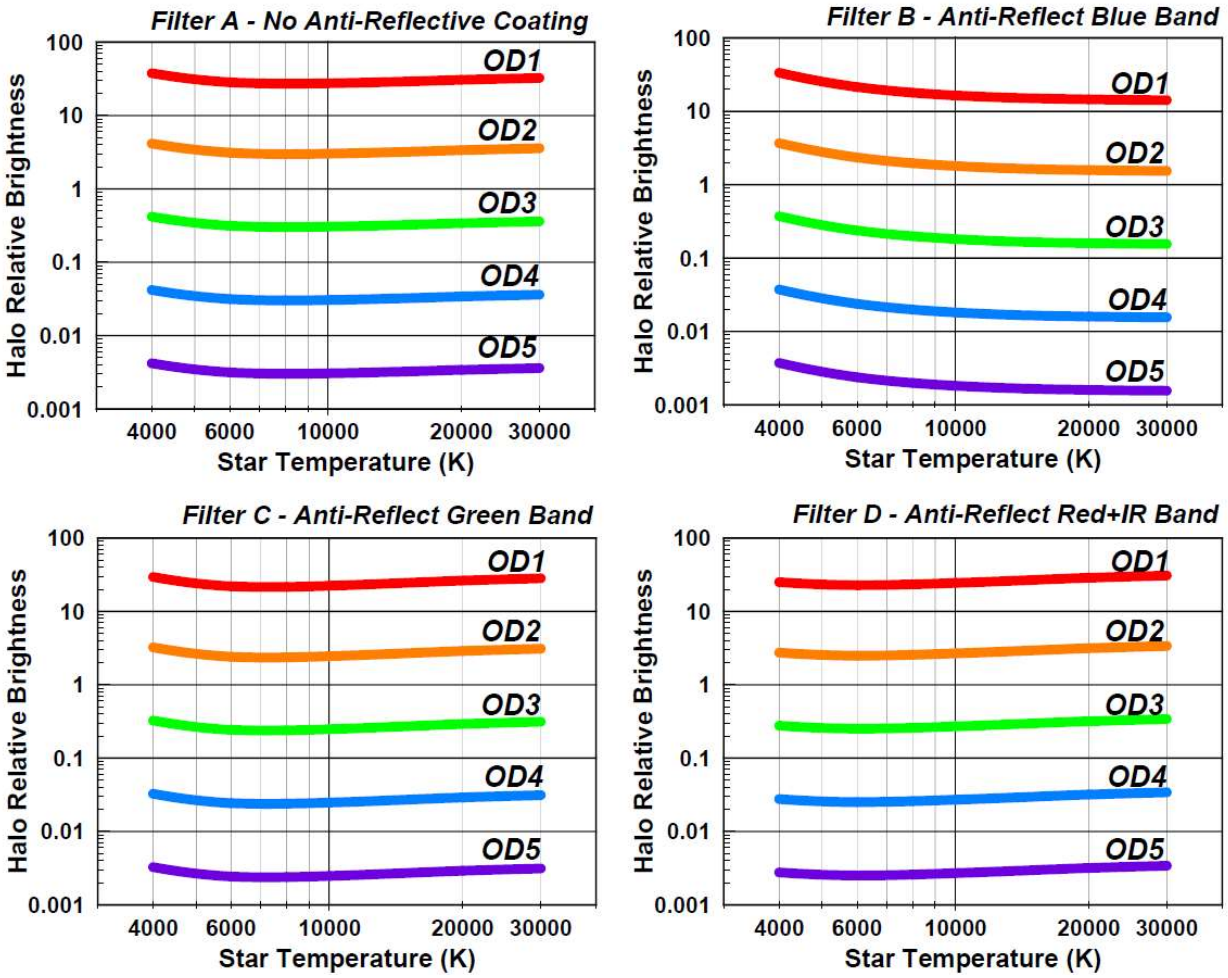

Figure 21 Simulated Halo Brightness Comparison

Looking now at all four filter plots together, it is very evident that off-band blocking is the dominant filter performance characteristic affecting halo brightness. For every integer value increase in OD (i.e. from 1 to 2, 2 to 3, etc.), the halo brightness goes down by a factor of 10. Thus, my observation #3 is confirmed by this simulation.

The final observation to verify from the simulation results is #4, that anti-reflective coatings can help to reduce halos, but they are not the main filter characteristic driving halo brightness. Although hard to tell from the plots in Figure 21 for Filters C and D, it is clear for the Filter B plot that the anti-reflective coating is affective at reducing the halo brightness compared to the filter without anti-reflective coatings (Filter A). To help visualize the impact of the anti-reflective coating on halo brightness I have plotted the relative halo brightness of each filter compared to Filter A. The resulting graph is shown in Figure 22. The simulation suggests that anti-reflective coatings in the green and red bands have only a moderate impact on halo brightness, with reduction values in the 10-20% range. Coatings in these bands are most effective on cool stars, which may not be that useful if the observing bias I noted above is universal amongst filter users. Anti-reflective coatings in the blue band are predicted to be significantly more effective at reducing halo brightness, especially on hot stars. In terms of "bang for your buck" it makes sense

that if a filter manufacturer was willing to invest in adding an anti-reflective coating to their filter, it would be best if they focused on coatings in the blue part of the spectrum. That said, even if the filter had non-reflective coatings in all three bands, that would not be as effective as improving the off-band blocking.

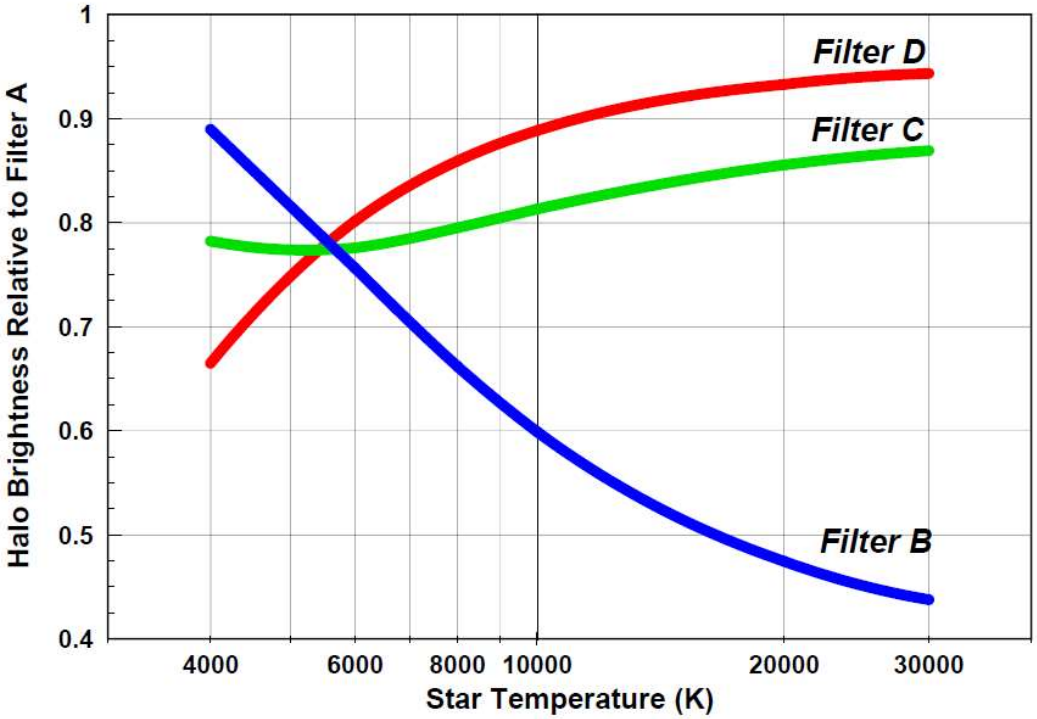

Figure 22 Impact of Anti-Reflective Coating on Simulated Halo Brightness

9.0 Conclusions

The following conclusions have been drawn from the experiments and analysis performed on the topic of filter induced star halos:

1. Filter induced artifacts are caused both by reflections from the exterior surfaces of the filter, and reflections occurring within the filter. Artifacts commonly identified as halos are primarily due to intra-filter reflections. Although the results of my experiments support this conclusion, it was not until I did more research that I was able to understand what was going on. Of great assistance was the work done by Dr. Joseph Findlay while he was at the University of London. For his PhD thesis [5,6] he had to deal with similar imaging artifacts while analysing VISTA sky survey data. It was his work that helped me to finally make sense of all my observations.
2. The distance of the filter from the sensor does not impact the appearance of the halo. Its size is dependant on the thickness of the filter glass. This was an important observation for confirming that halos are primarily due to intra-filter reflections. Halo size will also vary depending on scope focal ratio.

3. The extent to which a halo is produced depends on the temperature of the star. Comparing stars with the same visual magnitude, very hot stars (>10,000K) and very cool stars (<5000K) will produce brighter halos than moderate temperature stars. Since filters are commonly used for imaging emission nebulae in star forming regions, there is likely an observing bias in the astrophotography community towards scenes containing young stars that are both hot and bright.
4. A filter's tendency to produce halos is highly dependant on its off-band blocking performance. From the 45 filters tested, all those with off-band blocking >OD4 had little or no discernable halo. For filters with blocking below OD4, secondary effects like filter reflectivity become more important.
5. Application of an anti-reflective coating on the camera side of the filter can help to reduce the appearance of halos, although the magnitude of the impact is less than increasing off-band blocking. An anti-reflective coating designed to operate in the blue part of the spectrum is most effective at reducing halo brightness, especially for very hot stars.

If you have any questions, please feel free to contact me.

Cheers!

Jim Thompson
(top-jimmy@rogers.com)

Appendix A - 20° Off-Axis Filter Spectral Reflectivity Plots

01 Antlia ALP-T

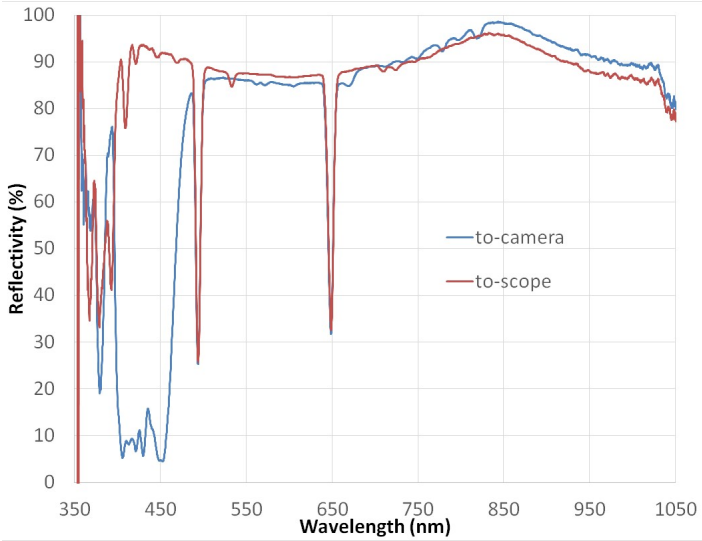

02 Arcturus UHC

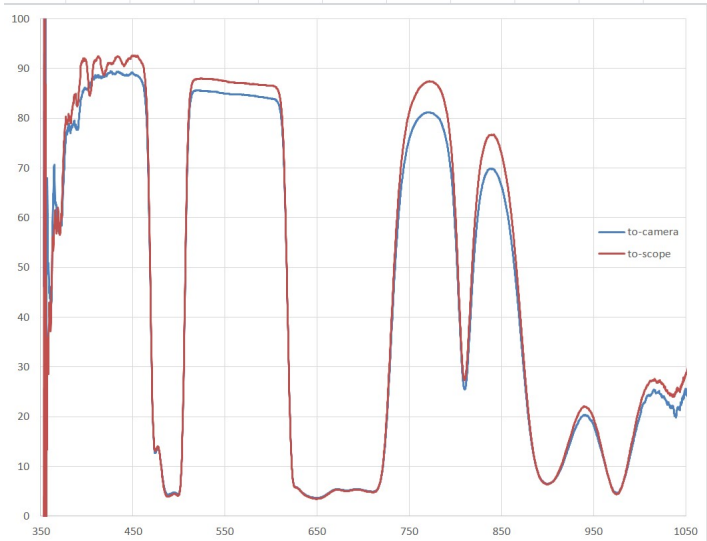

03 Askar 3nm Dual Narrowband

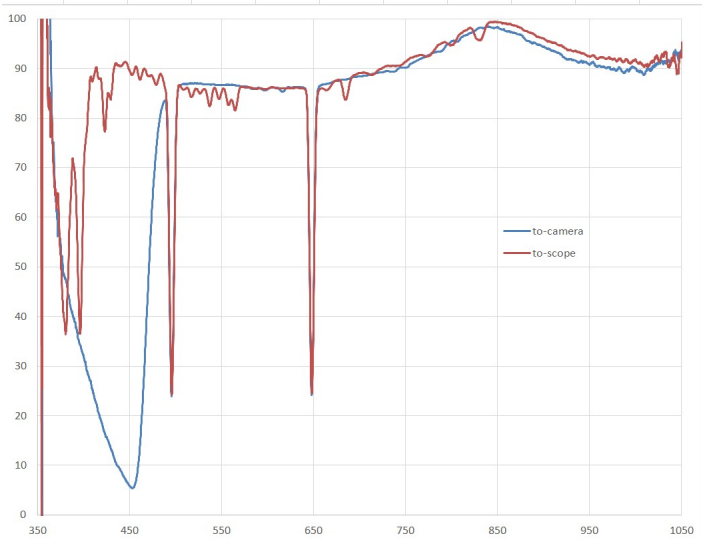

04 Astronomik Hbeta visual

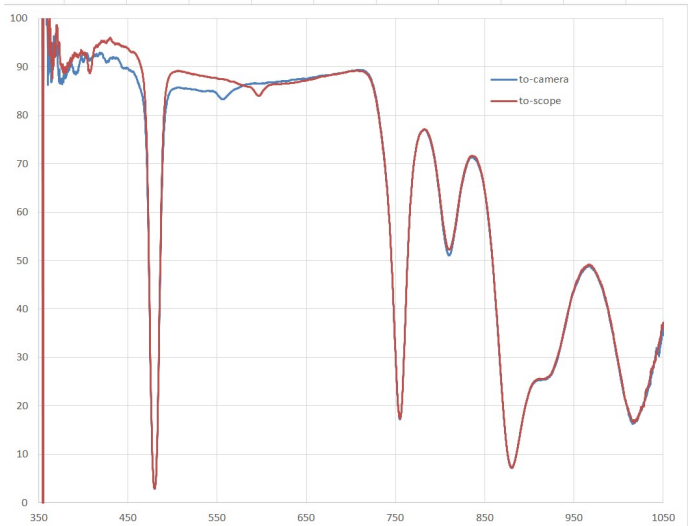

05 Astronomik IR Cut

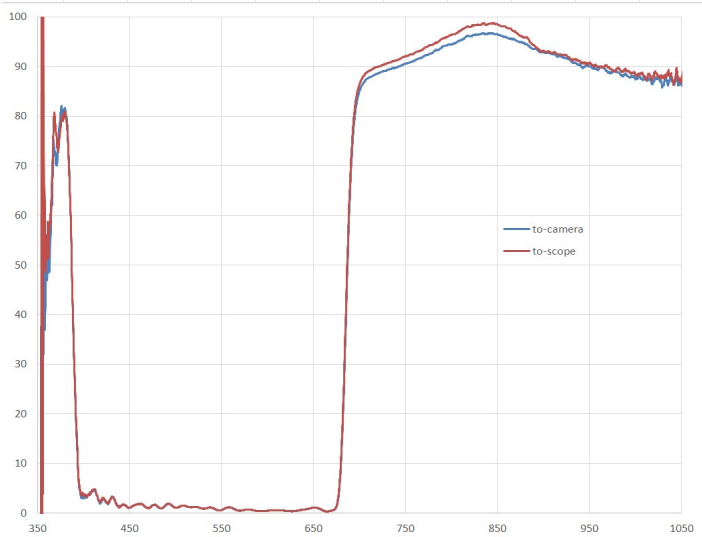

06 Astronomik OIII visual

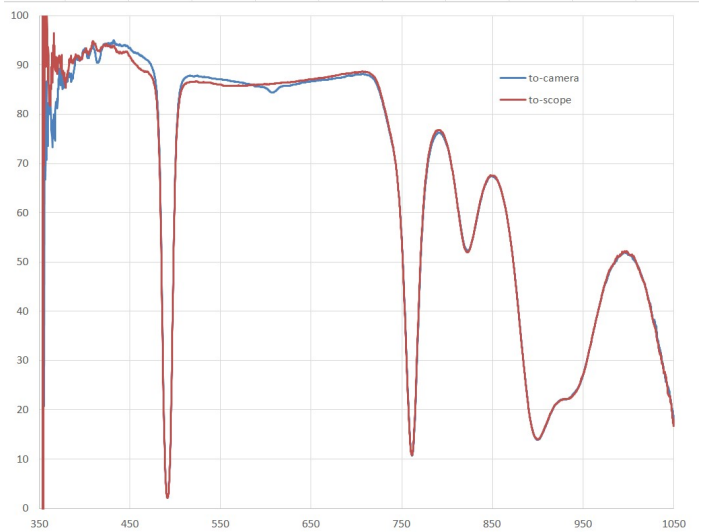

07 Astronomik ProPlanet 642

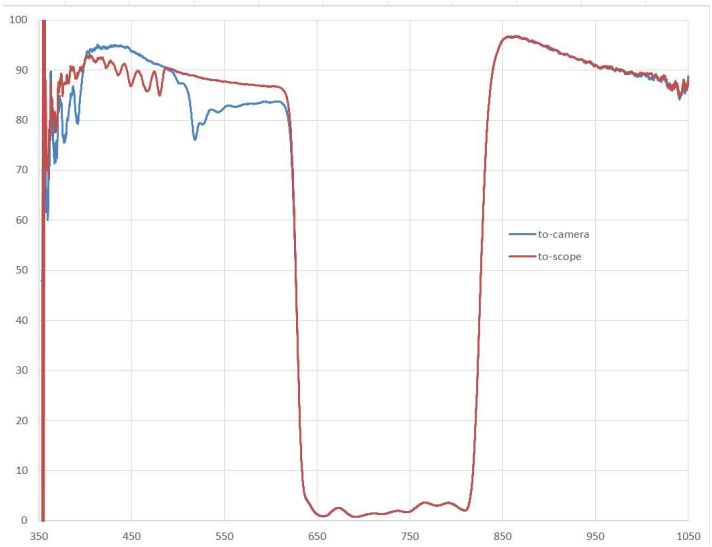

08 Astronomik UHC

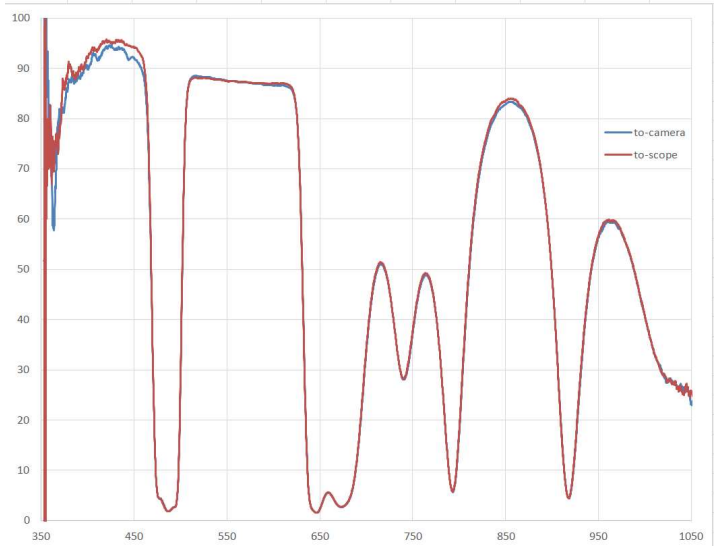

09 Baader IR Pass

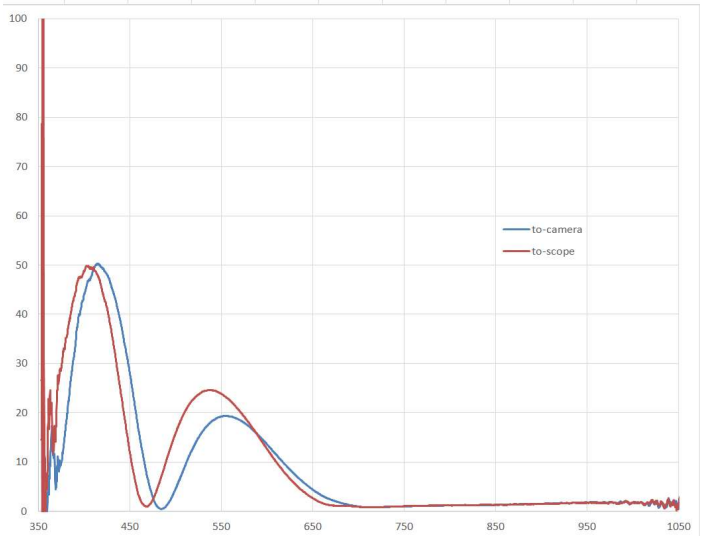

10 Baader UHC-S

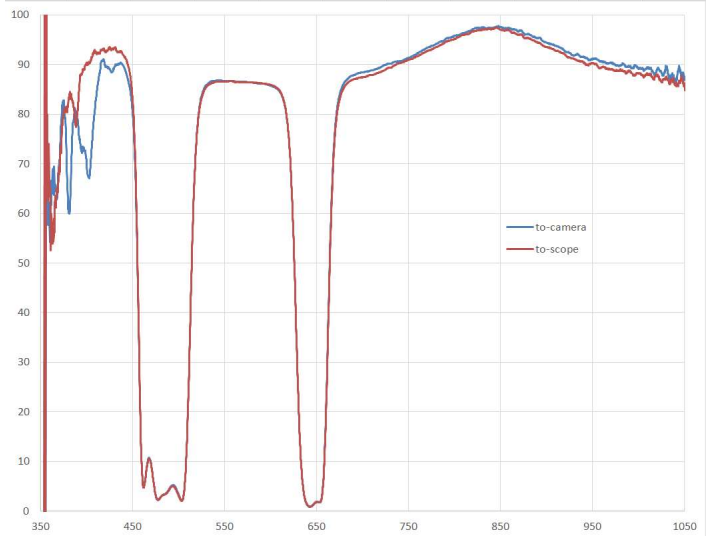

11 Baader UV/IR Cut

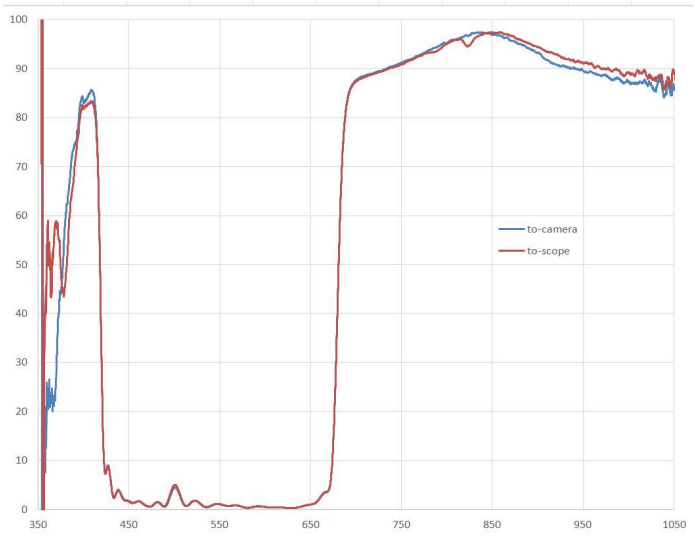

12 IDAS 6.0nm OIII

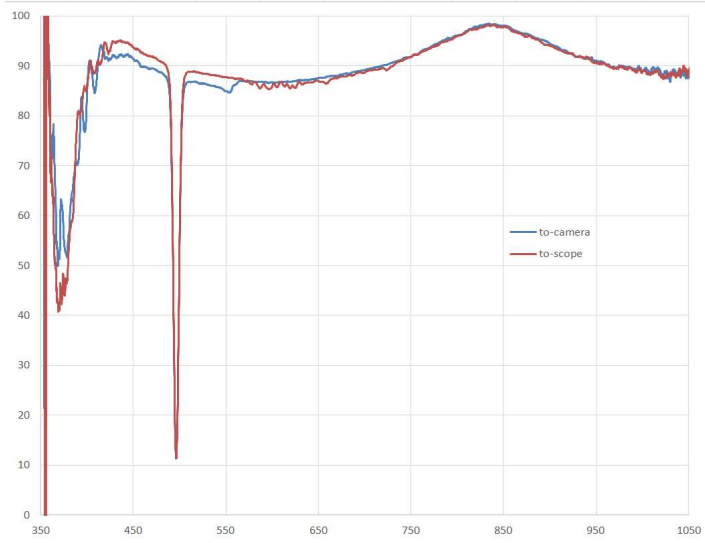

13 IDAS 6.8nm Halpha

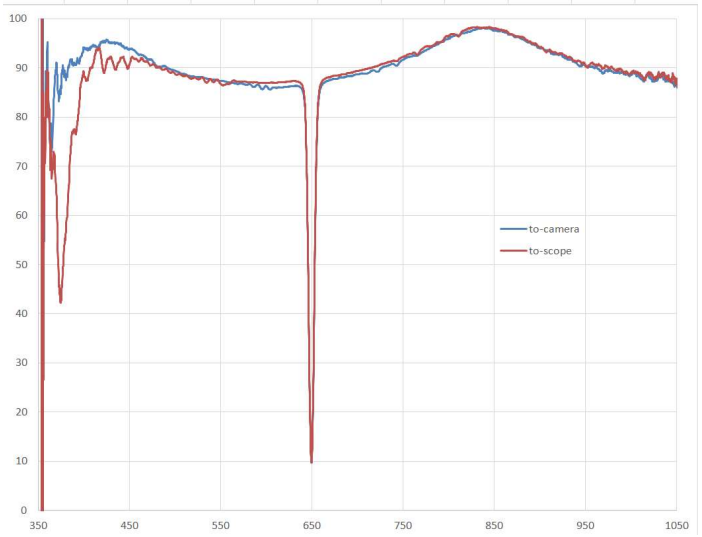

14 IDAS EAO1

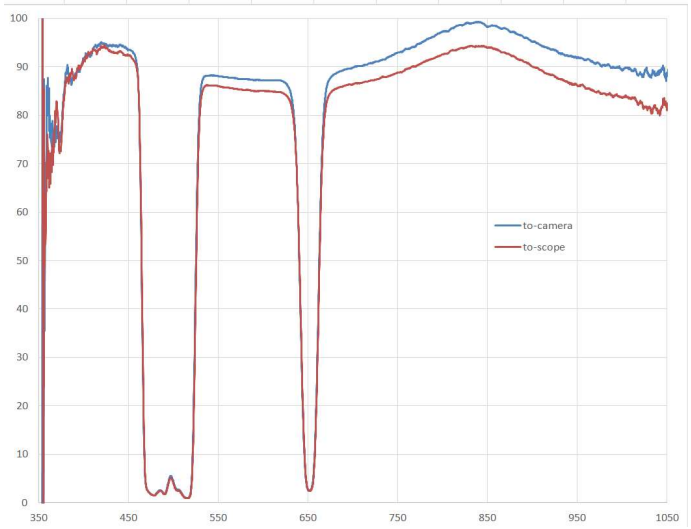

15 IDAS LPS-D2

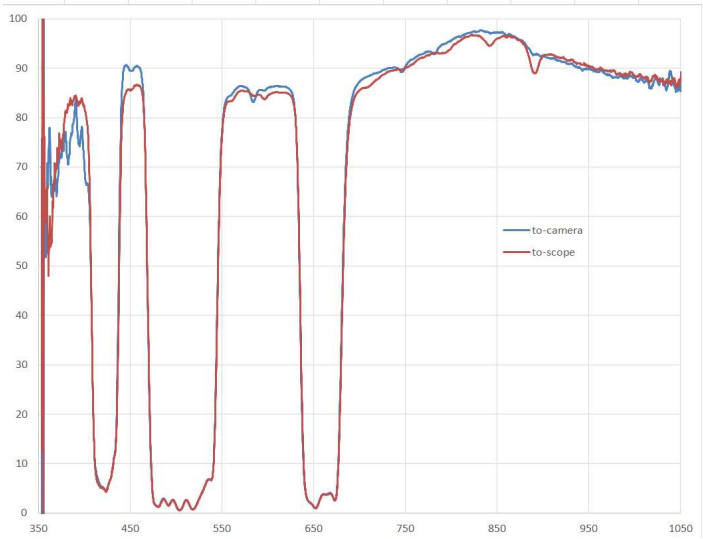

16 IDAS LPS-P2

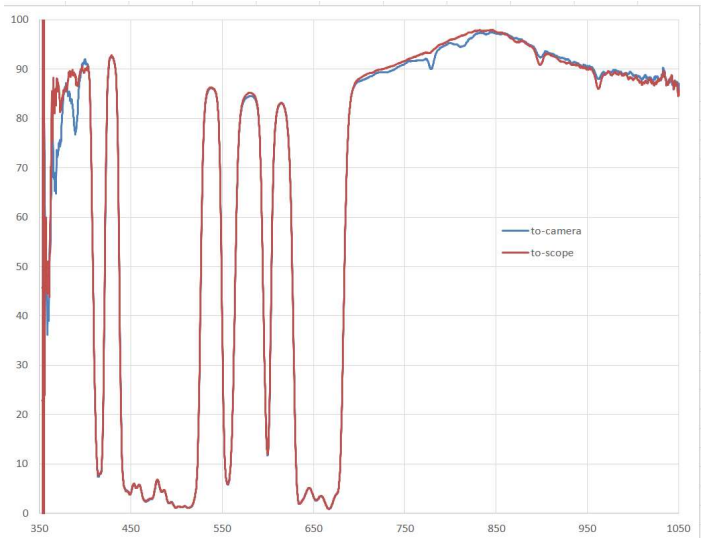

17 IDAS LPS-P3

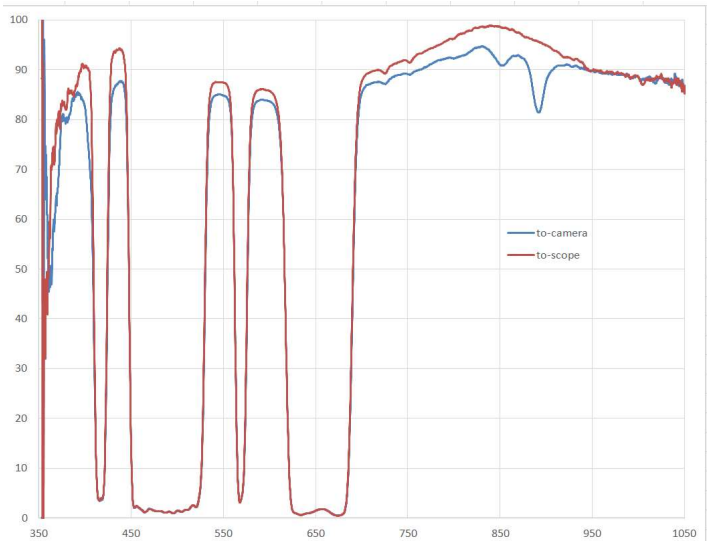

18 IDAS NB-1

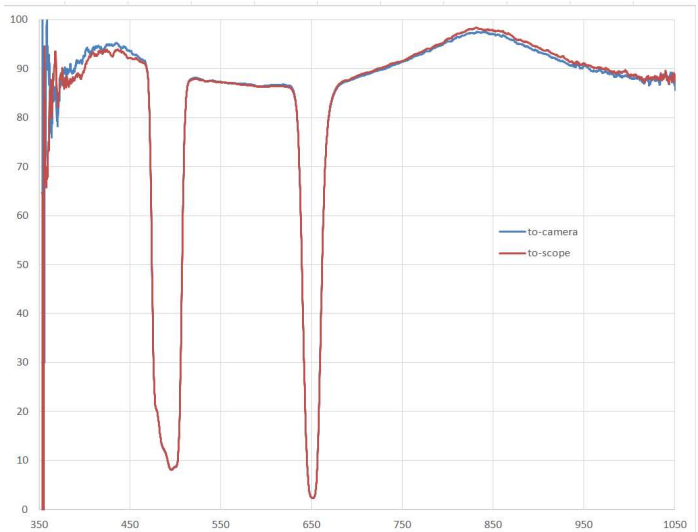

19 IDAS NB-2

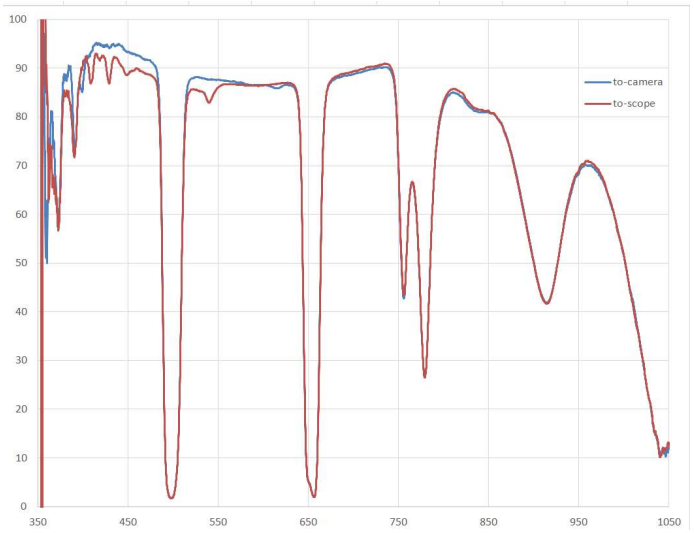

20 IDAS NB-3

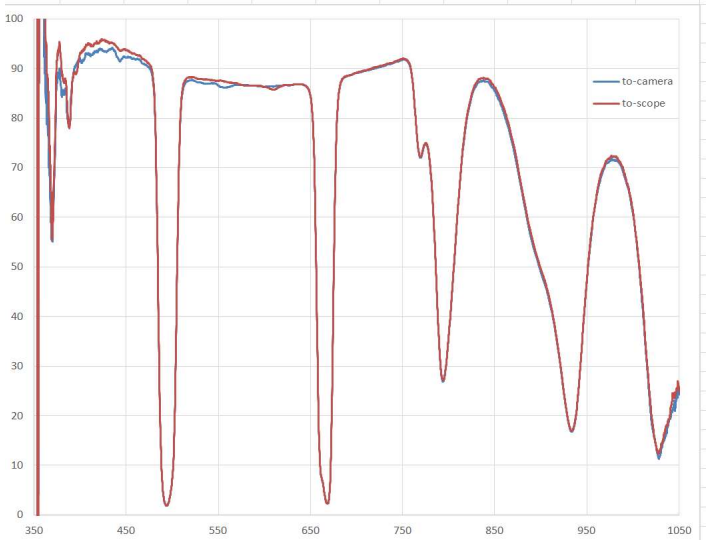

21 IDAS NBZ

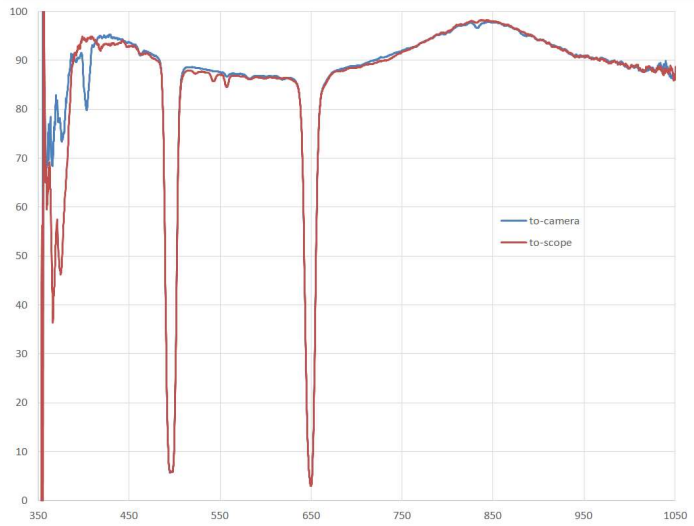

22 Lumicon Deepsky

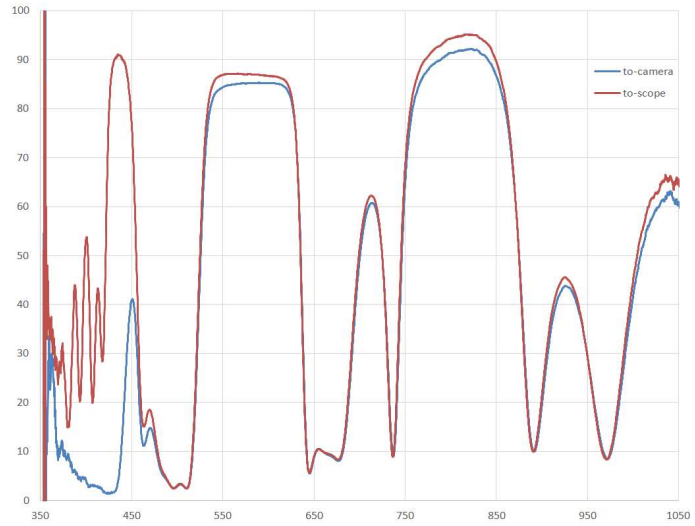

23 Meade Broadband

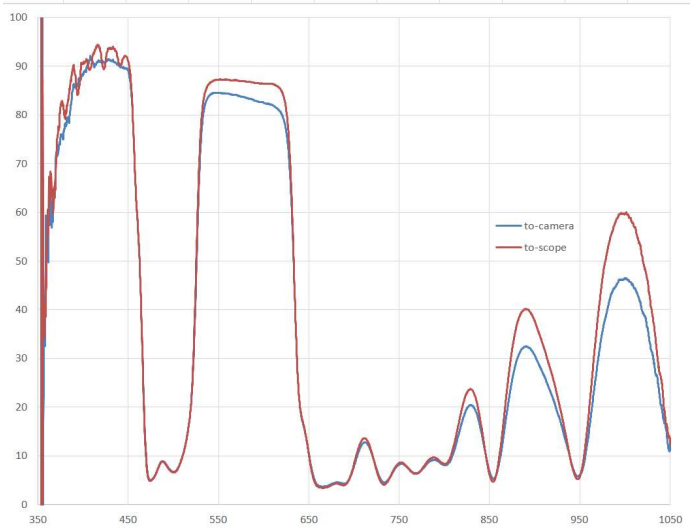

24 Meade OIII

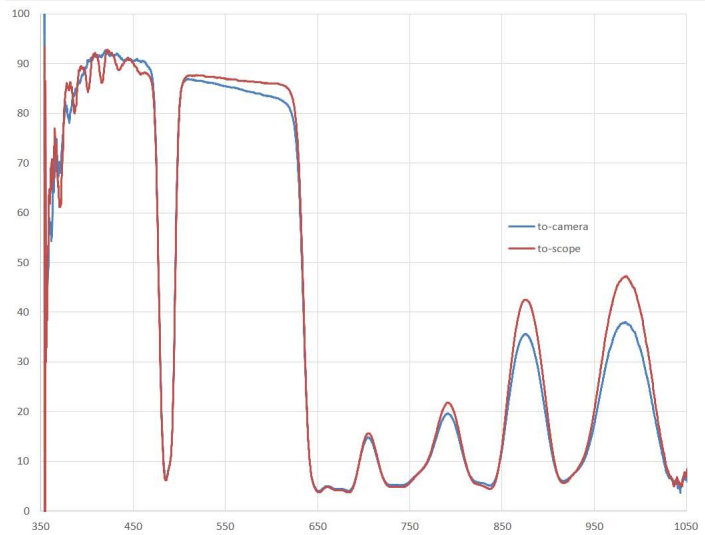

25 Omega 650BP10

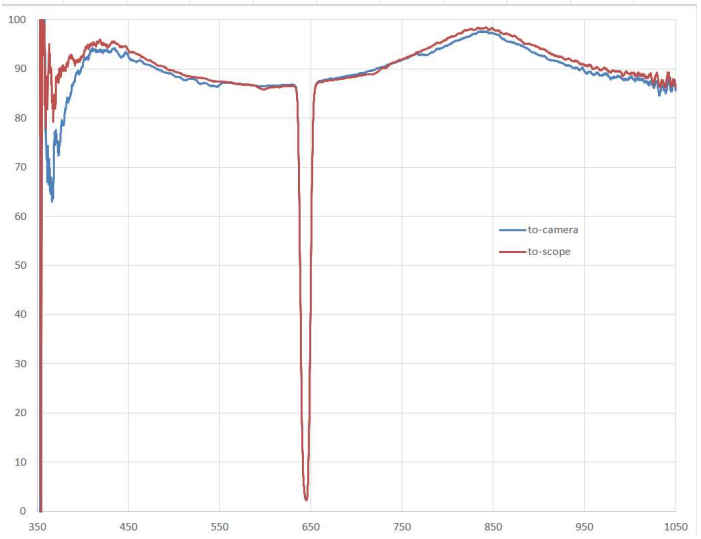

26 Omega BDRB

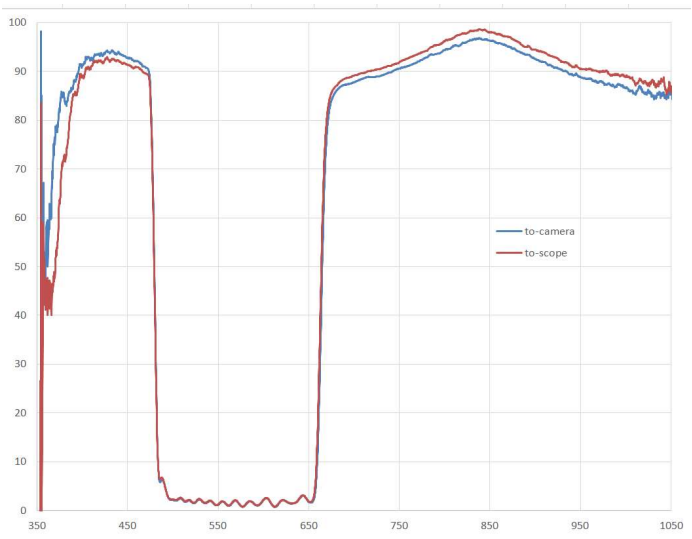

27 Omega NPB DGM Improved

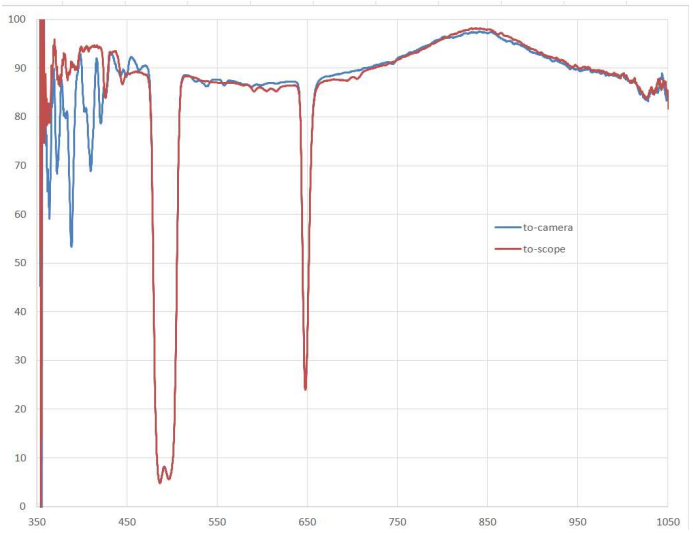

28 Omega XMV660/40

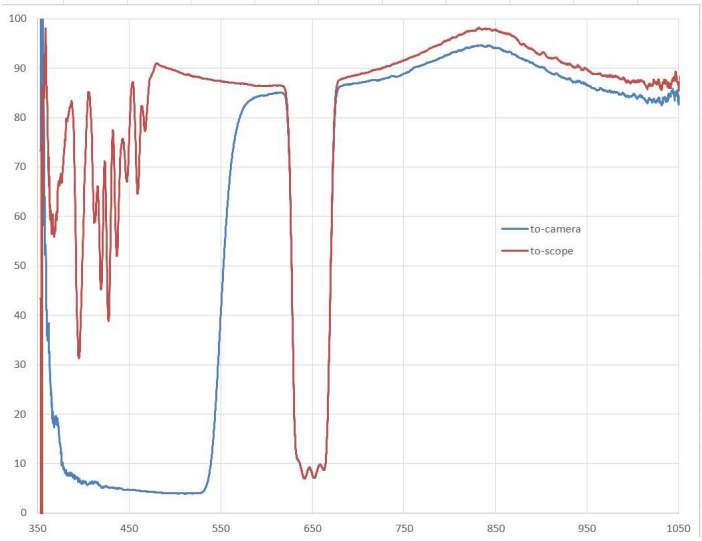

29 Optolong 3.0nm Halpha

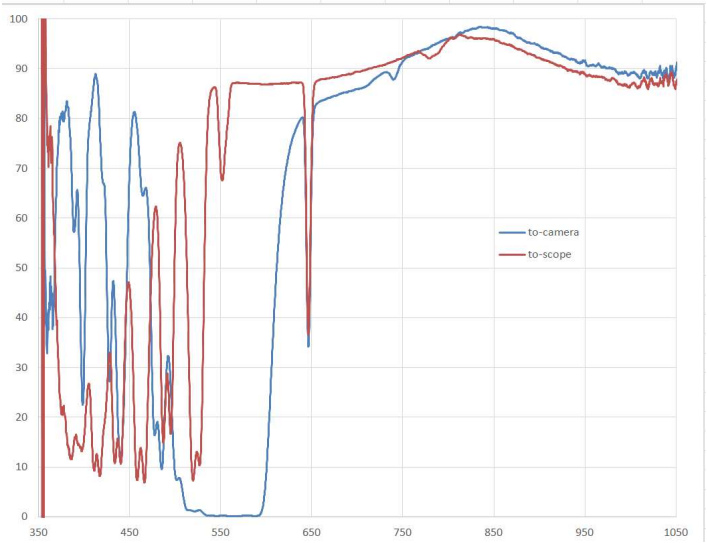

30 Optolong 3.0nm OIII

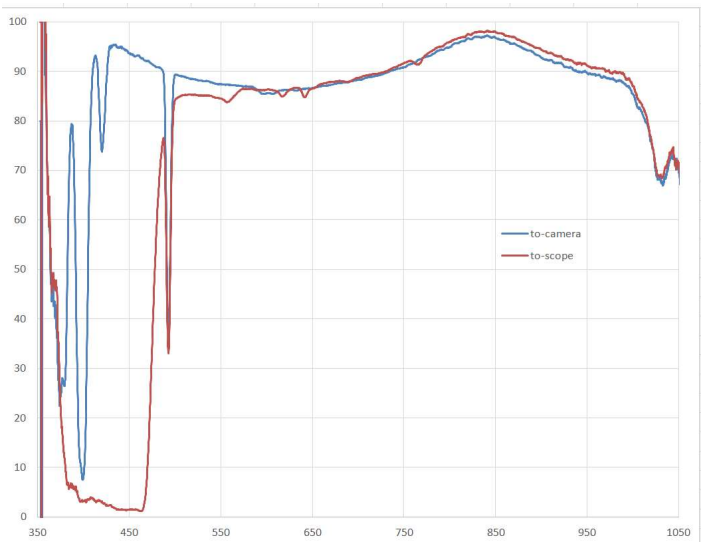

31 Optolong 3.0nm SII

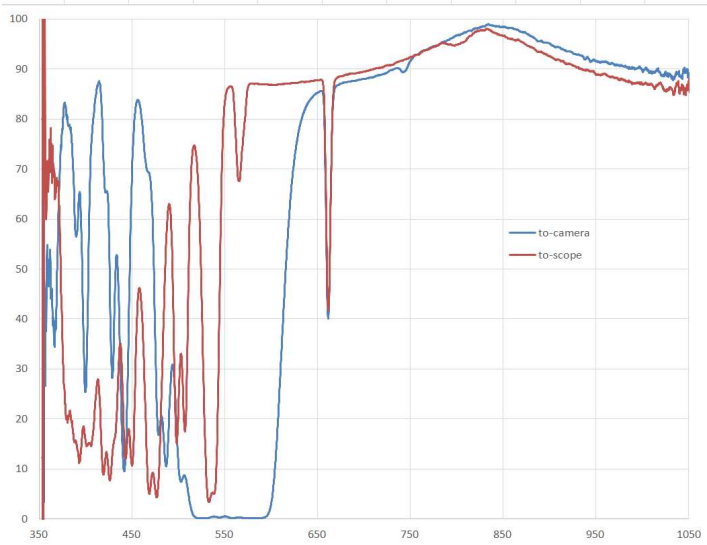

32 Optolong 6.5nm SII

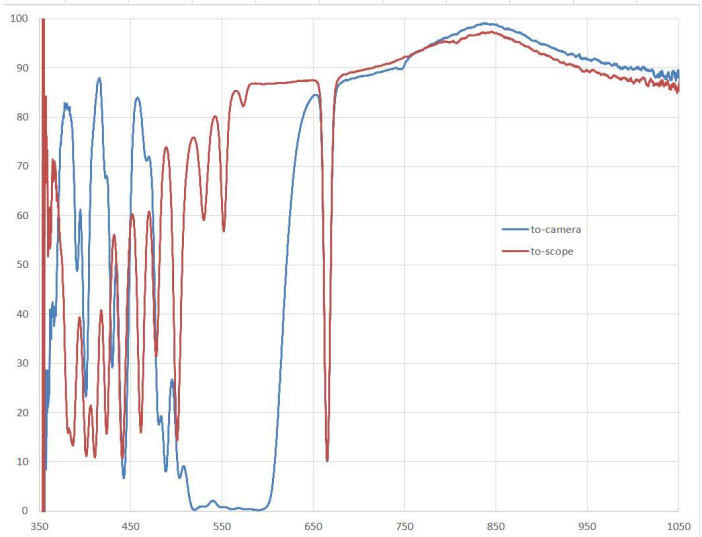

33 Optolong 7.0nm Halpha

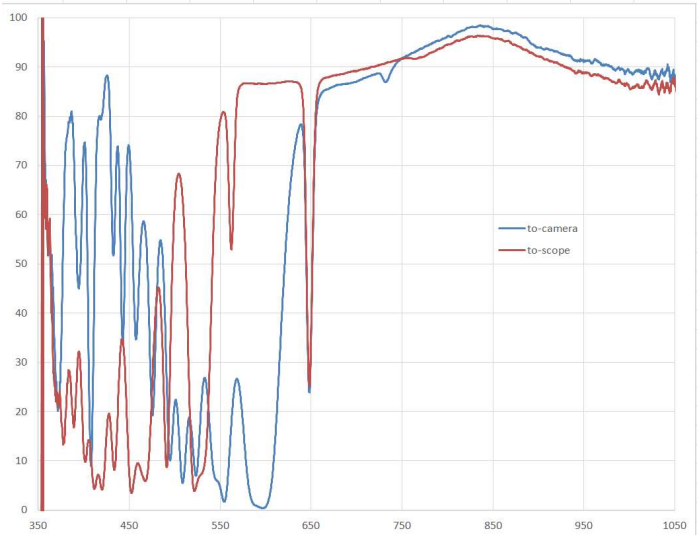

34 Optolong CLS

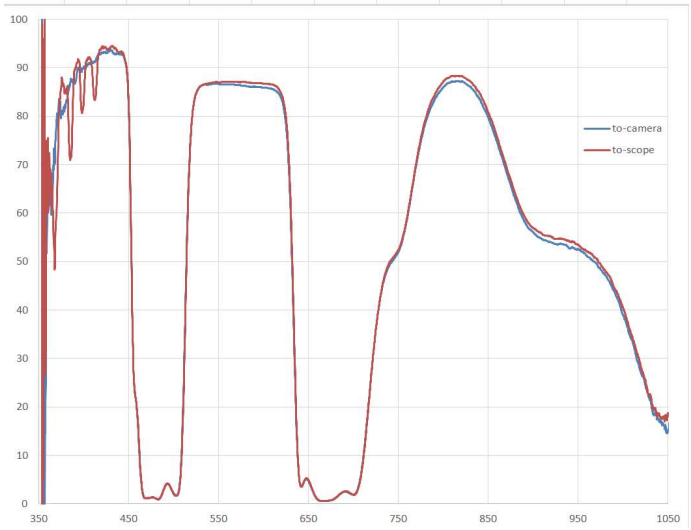

35 Optolong IR Cut

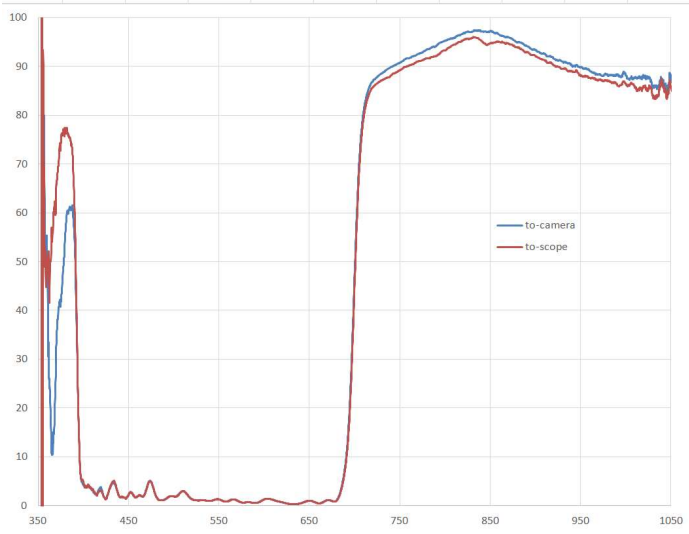

36 Optolong L-eNhance

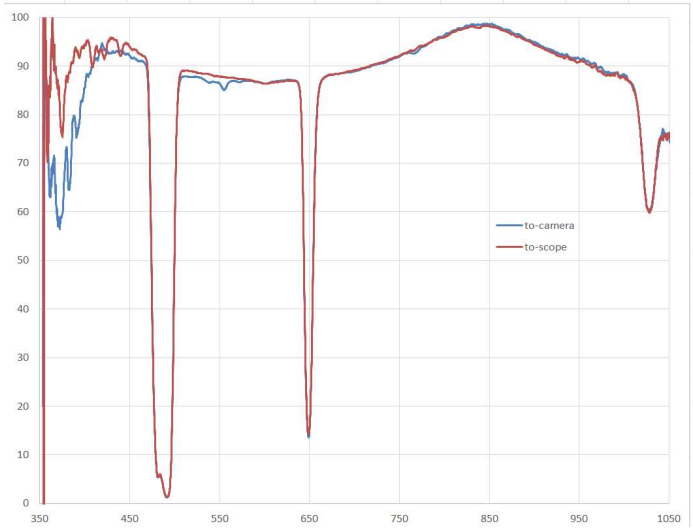

37 Optolong L-eXtreme

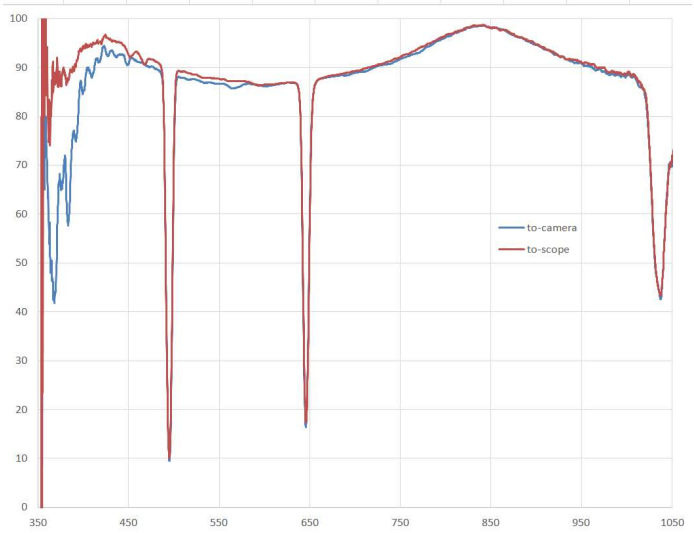

38 Optolong L-Pro

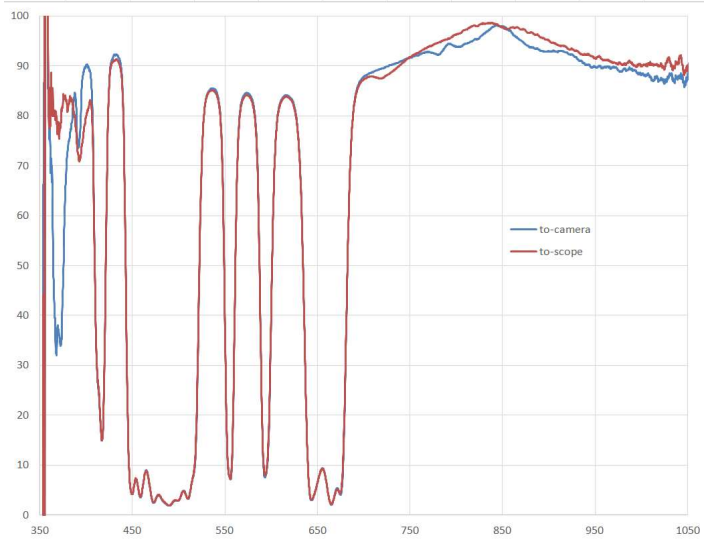

39 Optolong L-uLtimate

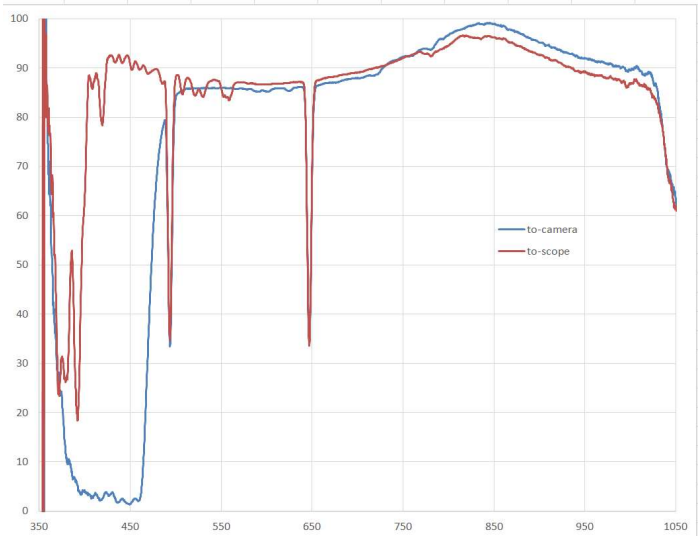

40 Optolong Nightsky Halpha

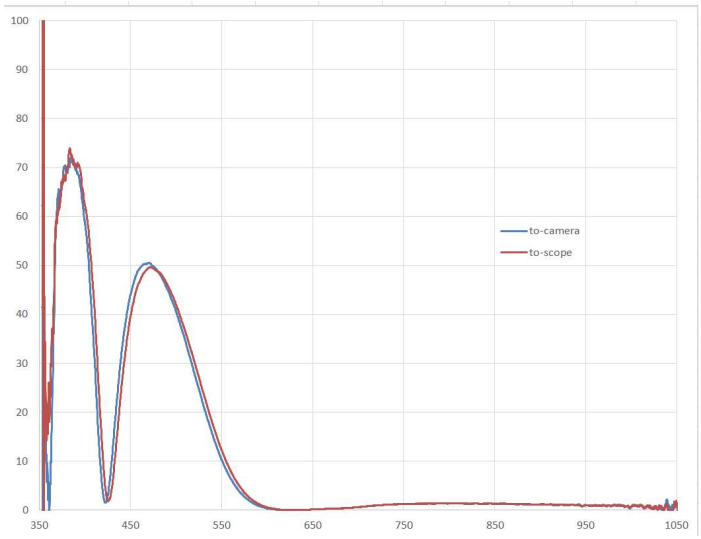

41 Optolong UHC

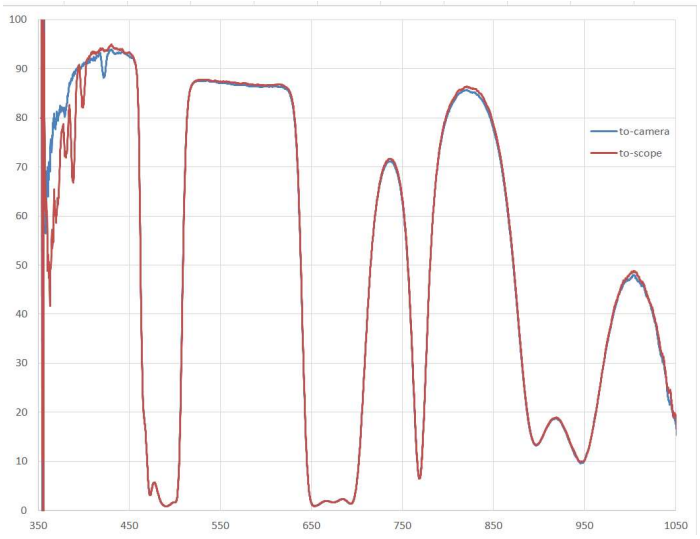

42 Radian Triad

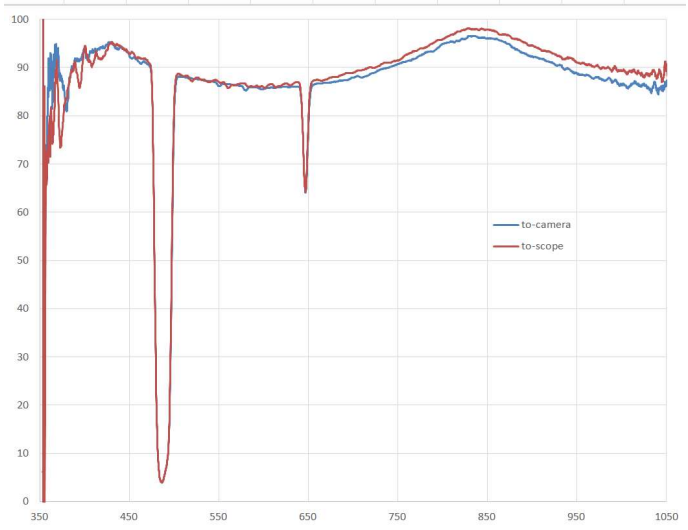

43 Radian Triad Ultra

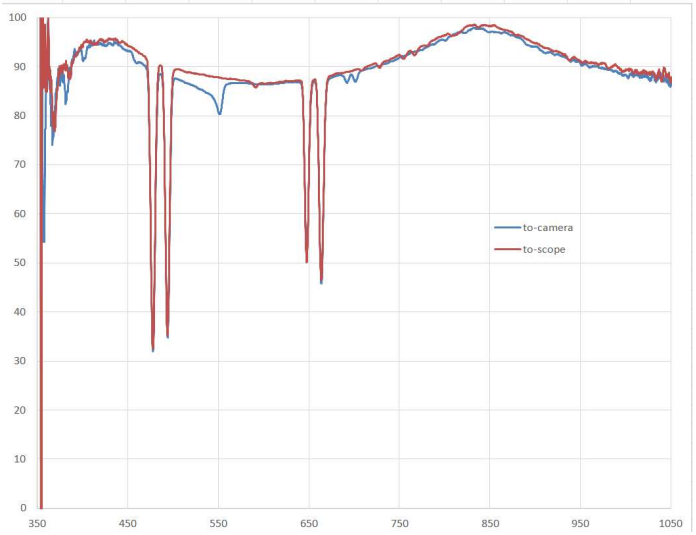

44 STC Duo-Narrowband

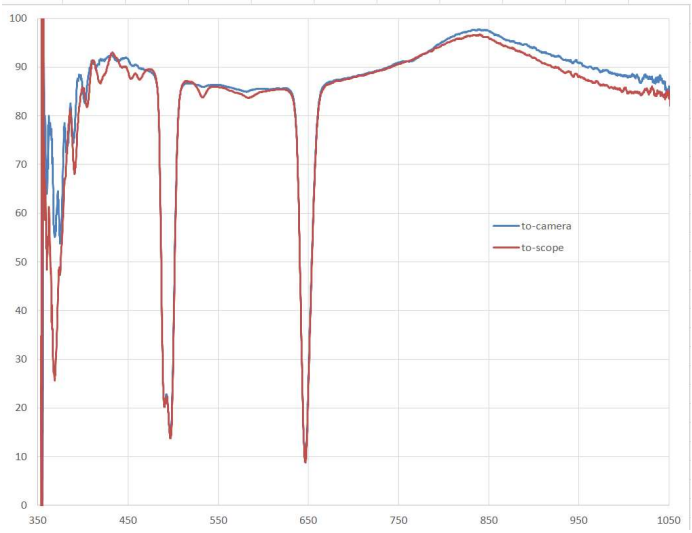

45 ZWO Duo-band

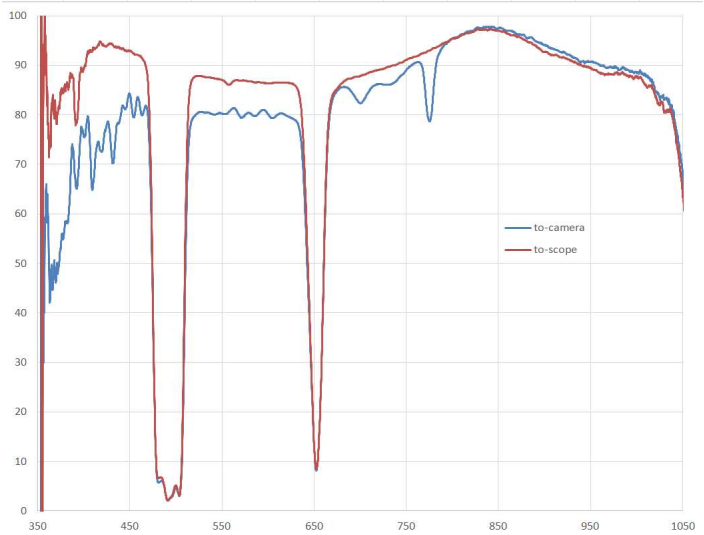

Appendix B – Summary Table of Measured Filter Properties

Filter Halo Testing Summary Table

Alphabet	Test		Luminous Transmissivity (IMX174M)	Mean Relative Reflectivity	Mean Off-Band Blocking	Primary Halo Relative Contrast	Mean Relative Reflectivity	Mean Off-Band Blocking	Primary Halo Relative Contrast	Mean Relative Reflectivity	Mean Off-Band Blocking	Primary Halo Relative Contrast	Primary Halo Relative Contrast	Visible Halo?	Notes
Order #	**Order #**	**Filter**		400-450 nm	400-430 nm	Blue Channel	500-600nm	550nm	Green Channel	800-900nm	800-900nm	Red Channel	Luminance		
		units	*[%]*	*[%]*	*[OD]*	*[%]*	*[%]*	*[OD]*	*[%]*	*[%]*	*[OD]*	*[%]*	*[%]*	*[y/n]*	
		estim. error	*+/- 0.2%*	*+/- 2%*	*+/- 0.1*	*+/- 0.1%*	*+/- 2%*	*+/- 0.1*	*+/- 0.1%*	*+/- 2%*	*+/- 0.1*	*+/- 0.1%*	*+/- 0.1%*		
1	1	Antlia ALP-T	2.3	9.1	4.0	0.06	85.8	4.7	0.51	96.9	4.0	0.08	0.29	n	faint blue, gradual fall-off, not defined
2	30	Arcturus UHC	37.4	88.5	2.1	0.25	79.7	3.7	0.62	42.9	0.4	0.52	0.50	y	faint all channels
3	45	Askar 3nm Dual Band	1.9	16.6	4.1	-0.02	86.4	>5	0.57	96.8	4.1	-0.16	0.24	n	gradual fall-off, not defined
4	33	Astronomik Hbeta visual	13.0	91.5	2.4	1.31	85.3	2.6	1.07	44.3	0.3	1.21	1.16	y	bright all bands
5	31	Astronomik IR Cut	65.2	2.6	0.3	0.15	0.9	0.0	0.26	95.4	2.5	0.09	0.19	n	gradual fall-off, not defined
6	34	Astronomik OIII visual	13.9	93.4	2.4	1.21	86.4	2.5	1.24	52.3	0.3	1.18	1.22	y	bright all bands
7	32	Astronomik ProPlanet 642	27.8	94.4	2.8	0.16	82.6	>5	0.29	71.1	1.0	0.53	0.32	y	red, faint blue green
8	2	Astronomik UHC	36.0	93.0	2.6	0.02	85.7	3.9	0.25	70.1	0.3	0.54	0.26	n	very faint red, gradual fall-off
9	16	Baader IR Pass	28.2	43.8	2.9	0.17	15.7	4.9	0.40	1.3	0.0	0.77	0.43	y	bright red, very faint other channels
10	35	Baader UHC-S	21.8	85.5	1.9	1.24	74.9	1.7	1.18	96.6	3.0	1.39	1.25	y	bright all channels, double
11	3	Baader UV/IR Cut	62.0	33.1	1.6	0.10	1.0	0.0	0.14	96.0	3.0	-0.17	0.05	n	gradual fall-off, not defined
12	18	IDAS 6.0nm OIII	1.7	91.1	3.7	0.14	85.9	3.3	0.45	97.0	3.4	-0.32	0.18	n	gradual fall-off, not defined
13	19	IDAS 6.8nm Halpha	1.5	94.6	4.1	-0.58	87.4	4.7	-0.13	96.7	3.6	-0.13	-0.25	n	gradual fall-off, not defined
14	36	IDAS EAO1	20.0	94.0	2.1	0.39	66.8	1.3	0.58	97.9	3.4	0.23	0.45	n	gradual fall-off, not defined
15	5	IDAS LPS-D2	33.3	37.9	1.8	0.59	48.4	0.0	0.70	96.1	3.0	0.07	0.52	y	all channels
16	17	IDAS LPS-P2	40.5	47.5	1.7	0.42	47.2	1.1	0.70	95.9	2.5	0.16	0.49	y	faint blue/green
17	4	IDAS LPS-P3	41.2	55.7	1.8	0.52	48.7	0.7	0.50	91.3	2.7	-0.04	0.37	y	faint green/blue
18	6	IDAS NB-1	12.5	94.3	2.9	0.48	81.6	2.7	0.96	96.1	3.2	0.18	0.65	y	all channels, bright green
19	37	IDAS NB-2	16.1	94.0	1.7	1.86	79.8	2.5	1.82	76.2	0.5	2.13	1.90	y	bright all chanels, double
20	38	IDAS NB-3	15.3	92.9	1.6	2.10	82.7	2.5	2.05	72.0	0.4	2.31	2.13	y	bright all chanels, double
21	7	IDAS NBZ	6.1	92.7	3.2	0.08	85.6	3.3	0.74	96.7	3.6	0.01	0.39	y	faint all channels
22	8	Lumicon Deepsky	38.5	8.6	1.9	0.28	64.6	0.9	0.89	68.8	0.8	0.32	0.59	n	gradual fall-off, not defined
23	21	Meade Broadband	45.1	90.5	2.2	0.47	65.5	0.8	0.89	18.1	0.1	0.51	0.69	y	bright all channels
24	20	Meade OIII	30.3	91.4	2.4	0.36	85.2	3.6	0.94	18.0	0.2	0.65	0.72	y	bright all channels
25	40	Omega 650BP10	2.3	93.3	4.6	-0.67	87.1	5.0	-0.26	95.8	4.3	0.51	-0.17	n	gradual fall-off, not defined
26	39	Omega BDRB	44.2	93.3	3.3	-0.21	1.7	0.0	0.39	95.2	3.5	0.01	0.14	n	gradual fall-off, not defined
27	23	Omega NPB DGM Improved	8.7	85.4	3.0	0.87	83.3	2.8	1.75	96.2	3.9	1.02	1.35	y	bright all channels, double
28	22	Omega XMV660/40	9.1	5.4	4.7	-0.61	42.7	>5	-0.09	93.1	3.4	0.22	-0.14	n	very faint red
29	27	Optolong 3.0nm Halpha	0.6	53.4	4.7	-0.52	1.3	>5	-0.36	97.0	3.9	0.28	-0.24	n	gradual fall-off, not defined
30	13	Optolong 3.0nm OIII	0.8	82.4	4.0	0.29	87.5	>5	0.76	95.7	3.6	0.35	0.54	y	poorly defined green
31	28	Optolong 3.0nm SII	0.6	53.0	4.7	-0.58	1.3	4.2	-0.15	97.5	3.7	0.18	-0.18	n	gradual fall-off, not defined
32	26	Optolong 6.5nm SII	1.5	51.0	4.7	0.21	1.7	4.8	0.32	97.5	3.4	0.48	0.33	n	gradual fall-off, not defined
33	12	Optolong 7.0nm Halpha	1.2	61.9	4.9	0.03	11.6	5.0	0.42	97.0	2.8	1.45	0.58	y	bright red, very faint other channels
34	42	Optolong CLS	38.2	91.9	1.9	0.58	74.9	1.8	0.76	75.7	0.6	0.46	0.64	y	all channels
35	41	Optolong IR Cut	66.9	2.9	0.6	0.31	1.2	0.0	0.57	96.0	2.5	0.11	0.39	n	gradual fall-off, not defined
36	9	Optolong L-eNhance	8.9	91.9	3.1	0.48	86.4	3.9	1.15	97.4	3.5	0.33	0.78	y	all channels, brightest green
37	10	Optolong L-eXtreme	3.2	91.4	3.9	0.17	86.7	4.5	0.82	97.2	3.6	0.12	0.48	y	all channels, brightest green
38	24	Optolong L-Pro	36.7	59.9	1.9	0.66	48.6	1.3	0.87	95.4	2.7	0.15	0.64	y	all channels
39	11	Optolong L-uLtimate	1.5	2.8	4.1	0.14	85.7	>5	0.69	97.7	4.0	0.08	0.40	y	faint all channels
40	25	Optolong Nightsky Halpha	38.0	25.7	2.9	0.26	14.2	4.5	0.39	1.3	0.0	0.67	0.43	y	red, faint blue green
41	43	Optolong UHC	34.5	92.3	2.4	0.65	79.9	3.1	0.98	62.7	0.3	0.82	0.86	y	all channels
42	29	Radian Triad	6.0	93.8	3.4	0.25	86.7	4.9	0.68	95.1	4.5	-0.32	0.32	n	faint green, not well defined
43	14	Radian Triad Ultra	3.9	94.1	3.5	0.32	85.8	>5	0.83	96.5	3.8	0.04	0.51	y	bright green, faint blue
44	44	STC Duo-Narrowband	6.9	90.6	2.8	0.25	84.5	2.5	0.75	96.2	3.0	0.12	0.47	n	gradual fall-off, not defined
45	15	ZWO Duo-band	11.9	76.0	3.0	0.11	72.9	3.2	0.52	96.5	3.4	0.00	0.29	n	gradual fall-off, not defined